© 2017. Published by The Company of Biologists Ltd | Development (2017) 144, 4406-4421 doi:10.1242/dev.155069

RESEARCH ARTICLE

Cell dynamics underlying oriented growth of the *Drosophila* wing imaginal disc

Natalie A. Dye[1,*], Marko Popović[2], Stephanie Spannl[1], Raphaël Etournay[1,3], Dagmar Kainmüller[1,4], Suhrid Ghosh[1], Eugene W. Myers[1,5], Frank Jülicher[2,5,*] and Suzanne Eaton[1,6,*]

ABSTRACT

Quantitative analysis of the dynamic cellular mechanisms shaping the *Drosophila* wing during its larval growth phase has been limited, impeding our ability to understand how morphogen patterns regulate tissue shape. Such analysis requires explants to be imaged under conditions that maintain both growth and patterning, as well as methods to quantify how much cellular behaviors change tissue shape. Here, we demonstrate a key requirement for the steroid hormone 20-hydroxyecdysone (20E) in the maintenance of numerous patterning systems *in vivo* and in explant culture. We find that low concentrations of 20E support prolonged proliferation in explanted wing discs in the absence of insulin, incidentally providing novel insight into the hormonal regulation of imaginal growth. We use 20E-containing media to observe growth directly and to apply recently developed methods for quantitatively decomposing tissue shape changes into cellular contributions. We discover that whereas cell divisions drive tissue expansion along one axis, their contribution to expansion along the orthogonal axis is cancelled by cell rearrangements and cell shape changes. This finding raises the possibility that anisotropic mechanical constraints contribute to growth orientation in the wing disc.

KEY WORDS: Ecdysone, Insulin, Culture, Imaginal disc, Proliferation

INTRODUCTION

The *Drosophila* larval wing imaginal disc is a powerful model system in which to study the integration of diverse types of regulatory cues for tissue growth. The wing disc is a relatively flat epithelial sac that grows during larval stages of development. As it grows, the rapidly proliferating cells on one side (the wing pouch) become pseudostratified, whereas cells on the other side become squamous. At pupariation, the wing pouch everts and flattens to assume the adult wing shape (Waddington, 1940).

The size and shape of the wing are largely, but not entirely, determined during the larval growth phase. At this stage, signaling centers located at the anterior-posterior (AP) and dorsal-ventral (DV) compartment boundaries not only establish patterns of gene expression but also promote growth (Beira and Paro, 2016; Hartl and Scott, 2014). Hedgehog produced in posterior cells signals across the AP boundary to stabilize the transcriptional activator Ci155 (Ci) and induce the expression of different target genes [i.e. *engrailed* and *decapentaplegic* (*dpp*)] at different distances (reviewed by Hartl and Scott, 2014). Dpp is itself a secreted signaling molecule that establishes a bidirectional gradient anteriorly and posteriorly, promoting patterned gene expression through graded phosphorylation of SMAD transcription factors (reviewed by Affolter and Basler, 2007). At the DV boundary, Wingless (Wg) expression and Notch signaling are maintained by a positive-feedback loop and together pattern the DV axis (Micchelli and Blair, 1999; Micchelli et al., 1997; Rulifson et al., 1996). Signaling from the AP and DV organizers is required for wing disc growth, even though cell proliferation is not especially concentrated near these regions (González-Gaitán et al., 1994; Milan et al., 1996; Schwank et al., 2011).

The orientation of tissue growth is strikingly non-uniform: marked clones strongly elongate along the proximo-distal (PD) axis of the adult wing (González-Gaitán et al., 1994; Resino et al., 2002; Baena-López et al., 2005; Mao et al., 2013; Worley et al., 2013; Heemskerk et al., 2014). In central regions of the larval wing pouch, the adult PD axis is generally orthogonal to the DV boundary. Signaling at organizer regions influences the growth orientation by establishing tissue-wide patterns of two planar cell polarity (PCP) systems, Fat and Core (Aw and Devenport, 2017). Both systems develop the same global pattern of planar polarity that presages the orientation of growth (Rogulja et al., 2008; Ambegaonkar et al., 2012; Sagner et al., 2012; Brittle et al., 2012). Perturbing Fat PCP or dominantly reversing the orientation of Core PCP both disrupt wing size and shorten it in the PD axis (Bryant et al., 1988; Clark et al., 1995; Mao et al., 2006; Merkel et al., 2014).

How the PCP patterns direct oriented tissue growth remains unclear. PD-oriented cell divisions clearly contribute to oriented tissue growth and are disturbed by genetic disruption of the Fat pathway (Baena-López et al., 2005; Mao et al., 2011). However, the extent to which oriented cell divisions or other dynamic behaviors (T1 rearrangements, cell shape changes or extrusions) quantitatively contribute to the tissue's growth pattern is unknown. Analytical tools now exist to describe tissue growth fully from cellular dynamics (Merkel et al., 2017; Etournay et al., 2016, 2015; Guirao et al., 2015), but such methods demand long-term time-lapse imaging at high spatial and temporal resolution. *In vivo* imaging has an insufficient time resolution (Heemskerk et al., 2014), necessitating the use of *ex vivo* culture. The achievement of prolonged *ex vivo* wing disc growth has proven difficult, even though the eversion process that imaginal tissues undergo at the onset of pupariation can be successfully replicated in culture (Fristrom et al., 1973; Milner, 1977; Aldaz et al., 2010). Importantly, in order to study properly the cellular dynamics underlying oriented growth, we require a culture condition that

[1]Max Planck Institute of Molecular Cell Biology and Genetics, Pfotenhauerstrasse 108, 01309 Dresden, Germany. [2]Max Planck Institute for the Physics of Complex Systems, Nöthnitzer Strasse 38, 01187 Dresden, Germany. [3]Unité de Génétique et Physiologie de l'Audition UMRS 1120, Département de Neurosciences, Institut Pasteur, 75015 Paris, France. [4]Janelia Farm Research Campus, 19700 Helix Dr, Ashburn, VA 20147, USA. [5]Center for Systems Biology Dresden, Pfotenhauerstrasse 108, 01309 Dresden, Germany. [6]Biotechnologisches Zentrum, Technische Universität Dresden, Tatzberg 47/49, 01309 Dresden, Germany.

*Authors for correspondence (julicher@pks.mpg.de; dye@mpi-cbg.de; eaton@mpi-cbg.de)

N.A.D., 0000-0002-4859-6670; M.P., 0000-0003-0934-5550; R.E., 0000-0002-2441-9274; E.W.M., 0000-0002-6580-7839; F.J., 0000-0003-4731-9185; S.E., 0000-0002-8319-284X

Received 19 May 2017; Accepted 5 October 2017

Development (2017) 144, 4406-4421 doi:10.1242/dev.155069

maintains the signaling from AP/DV organizers and global PCP patterns, and how *in vitro* culture affects these systems is completely unknown.

Insulin signaling regulates animal size in response to nutrition, and bovine insulin has been widely used to stimulate growth of explanted discs (Zartman et al., 2013; Handke et al., 2014; Mao et al., 2011, 2013; Legoff et al., 2013; Heller et al., 2016; Tsao et al., 2016; Strassburger et al., 2017). However, proliferation in insulin-cultured discs arrests within a few hours (Handke et al., 2014; Tsao et al., 2016); thus, clearly other signals are required for long-term growth. One such missing signal could be ecdysteroids, a family of steroid hormones produced by the ring gland in arthropods with well-characterized functions in regulating major developmental transitions (Kozlova and Thummel, 2000). A peak of 20-hydroxyecdysone (20E) and related hormones at the larval-to-pupal transition induces pupariation and imaginal disc eversion (Fristrom et al., 1973; Milner, 1977). This peak is preceded by a smaller elevation in hormone levels that starts in the mid-third instar (Kozlova and Thummel, 2000; Lavrynenko et al., 2015). The levels of ecdysteroid at this stage are about 4% of the peak concentration. Several lines of evidence now suggest that these lower concentrations promote imaginal growth and development during larval stages (Bodenstein, 1943; Brennan et al., 1998, 2001; Mirth et al., 2009; Delanoue et al., 2010; Mitchell et al., 2013; Herboso et al., 2015).

Here, we show that physiologically low levels of 20E, in the absence of insulin, extend the proliferation of explanted wing discs compared with insulin alone. Transcriptome sequencing reveals that 20E is required in culture for the normal expression of numerous genes involved in wing patterning, whereas insulin promotes a strong but transient anabolic growth response. Genetic perturbations *in vivo* confirm that 20E has widespread effects on morphogen signaling and PCP in the larval wing, highlighting the importance of including 20E in culture media for replicating *in vivo* growth patterns. We exploit this improved system to perform live imaging and apply recently developed tools for decomposing tissue growth into cellular contributions (Merkel et al., 2017; Etournay et al., 2016, 2015). Our analysis indicates that divisions alone are insufficient to account quantitatively for the anisotropy of tissue; cell rearrangements and cell shape changes play an equally important role. This work inspires new directions for exploration into the regulation of tissue size and shape.

RESULTS

Low levels of 20E stimulate cell division in cultured wing discs

We directly tested the ability of low levels of 20E, with or without insulin, to maintain proliferation in explants from mid-third instar larvae [96 h after egg laying (AEL)]. *In vivo*, these discs would continue to proliferate for another 24 h (pupariation at ∼120 h AEL). We monitored the numbers of phospho-histone H3-positive proliferating cells in freshly explanted discs, and compared them with discs cultured in the absence of hormones, or in the presence of 20 nM 20E, 1 µM insulin, or both hormones (Fig. 1A,B). In the absence of any hormones, the number of mitotic cells per area (proliferation index) is dramatically reduced by 4 h and negligible by 9 h (Fig. 1Ai,Bi), consistent with previous work (Zartman et al., 2013; Handke et al., 2014). In the presence of insulin, the proliferation index drops to half that of freshly explanted discs after 4 h and continues to decline thereafter (Fig. 1Aii,Bii). These indices quantitatively agree with those of previous analyses of insulin-culture discs (Handke et al., 2014).

Strikingly, in the presence of 20E alone, the proliferation index is similar to that of insulin-cultured discs at 4 h, but instead of declining thereafter, the index actually increases (Fig. 1Aiii,Biii). From 9-16 h after explant, the same density of mitotic nuclei is found in 20E-cultured discs as in freshly explanted discs. Proliferation even extends to 24 h, albeit at a lower density than between 9-16 h. By 24 h, the overall morphology becomes somewhat abnormal (Fig. S1), perhaps reflecting the fact that components of the extracellular matrix come from the fat body *in vivo* (Pastor-Pareja and Xu, 2011).

The simultaneous addition of both hormones promotes proliferation mildly better than either alone for 4 h; but by 9 h, proliferation declines, as in the presence of insulin alone. Unlike in any other condition, however, the morphology of discs cultured for 9 h in insulin +20E becomes abnormal, as visualized by the cell area distribution in Fig. 1C. Proliferation is not significantly improved by adjusting 20E concentration (Fig. S1). Thus, under these explant conditions, the response triggered by the combined addition of hormones is incompatible with long-term proliferation with normal morphology.

Transcriptional responses to 20E and insulin in explanted wing discs

To assess the consequences for gene expression of culturing under different hormonal conditions, we sequenced the transcriptomes of freshly explanted discs (96 h AEL), discs cultured without hormones for 4 h, and discs cultured for 4 or 9 h in either 20E or insulin alone. Relative to freshly explanted discs, the expression of 1604 genes goes down and 1409 genes goes up after 4 h of culture without hormones. Changed expression of 1911 genes (63%) could be prevented, at least transiently, by the addition of either 20E or insulin. Some genes responded to both 20E and insulin, whereas others were hormone specific.

Fig. 2 shows the size and overlap of the hormone-responsive gene sets. Comparing the transcriptional response to insulin at 4 and 9 h reveals that it is largely transient (Fig. 2A), consistent with the decreased proliferative response to insulin by 9 h (Fig. 1Aii,Bii). In contrast, although 20E regulates a smaller subset of genes, its effects are longer lasting (Fig. 2A). A subset of genes is regulated by either hormone (Fig. 2B). Maximum overlap (353 genes) occurs at time points when each hormone supports maximum proliferation (insulin at 4 h, 20E at 9 h). This overlap represents 22% of all insulin-regulated genes and 60% of 20E-regulated genes.

The transcriptional response to insulin that we observe in the wing disc is consistent with the results of many previous studies characterizing nutrient-dependent gene expression in other contexts (Fig. 3, Figs S2, S3) (Gershman et al., 2007; Teleman et al., 2008; Li et al., 2010). Genes induced by insulin are significantly enriched in gene ontology (GO) terms describing translation and ribosome biogenesis, cell cycle/DNA replication, and mitochondrial biogenesis (Fig. 3, Fig. S2). Conversely, insulin reduces the expression of genes involved in autophagy and cell death (Fig. 3, Fig. S6C). By 9 h of culture, however, the response of >70% of all insulin-regulated genes either weakens or disappears. This transient-responding group (Fig. 3Aii,B) includes many previously identified targets of the TOR pathway and the transcription factor FoxO, which lie downstream of insulin signaling (Fig. S3). The only enriched GO categories in the stably regulated genes (∼30% of total) describe oxoacid metabolic reactions (Fig. 3Ai).

To determine whether the decline in the transcriptional response to insulin reflects a loss of sensitivity to the hormone during culture, we examined two readouts of pathway activity. Binding of insulin to its receptor activates phosphoinositide 3-kinase (PI3K), activity of which can be monitored with a reporter that binds to the enzyme's product, phosphatidylinositol (3,4,5)-trisphosphate [PtdIns(3,4,5)P3 or PIP3]. Even after 9 h of culture, we observe

Development (2017) 144, 4406-4421 doi:10.1242/dev.155069

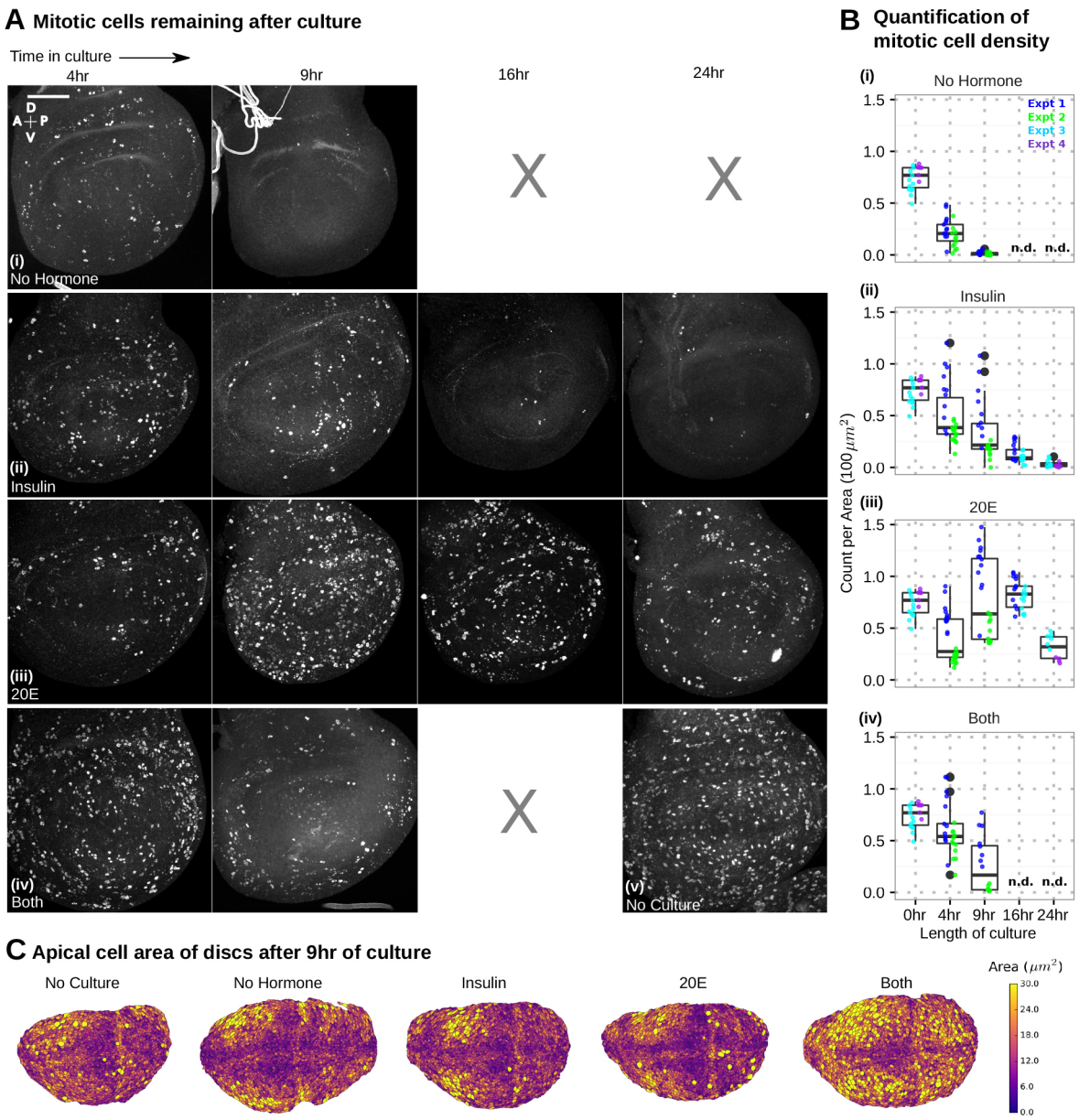

Fig. 1. 20E is sufficient to stimulate prolonged cell division in cultured wing discs. Wing discs (96 h AEL, mid-third instar) were cultured and then stained with phospho-Histone H3 to detect mitotic nuclei at the indicated time points. (A) Representative images of discs that were given no hormone (i), 5 µg/ml insulin (ii), 20 nM 20E (iii) or both (iv). In (v), an uncultured disc from 96 h AEL (0 h) is shown for comparison. (B) Quantification of PH3 density in the pouch (number of nuclei per 10×10 µm^2). For ease of comparison, the same data from uncultured discs are included in all graphs (labeled as 0 h). Each dot represents a single disc, color-coded by the date of experiment; box plots summarize all data per condition. n.d., not determined. (C) Cells of the wing pouch, color-coded by apical cell area, after 9 h of culture. Scale bar: 50 µm.

strong membrane localization of the reporter (Fig. S4), suggesting that PI3K activity is stable. We also examined the intracellular localization of FoxO, a transcription factor that is phosphorylated and retained in the cytoplasm during insulin signaling. Even after 9 h, insulin maintains robust nuclear exclusion of FoxO (Fig. S5). This is surprising because we found that ostensibly FoxO-induced targets that repress growth (i.e. the translational repressor 4E-BP; also known as Thor) are reactivated after 9 h of insulin culture (Fig. S3B). Thus, the retention of FoxO in the cytoplasm is not sufficient for maintaining the insulin-dependent transcriptional state or growth in the wing disc. Additional insulin-independent transcriptional regulators must affect these growth-inhibitory FoxO target genes.

About 22% of insulin-responsive genes are also regulated by 20E, at least after 9 h of culture. Both hormones repress genes involved in DNA-damage response and cell death and induce genes involved in DNA replication (Fig. S6). Amongst the shared targets, we found a subset involved in protein synthesis and nutrient transport, as well as some previously identified TOR- and FoxO-responsive genes (Figs S6 and S3). For example, 4E-BP is ectopically activated when explanted discs are cultured without hormone, but can be repressed either by insulin (at 4 h) or 20E. These data suggest that there could be crosstalk between the 20E- and insulin-signaling pathways and are consistent with a previous report that 20E can affect 4E-BP levels in wing discs *in vivo* (Herboso et al., 2015).

Development (2017) 144, 4406-4421 doi:10.1242/dev.155069

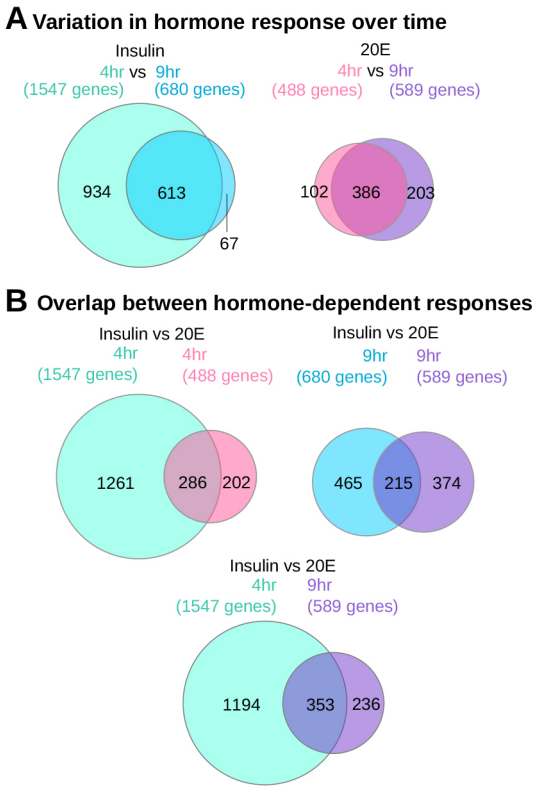

Fig. 2. Size and overlap of the transcriptional responses to 20E or insulin. Transcriptomes of wing discs cultured in either 20E or insulin were sequenced and compared with those of uncultured discs (96 h AEL) and discs cultured without any hormone (for 4 h). A gene was classified as hormone dependent if its levels changed upon culture without hormone and responded in the correct direction (more similar to uncultured levels) when cultured with hormone. (A) Total number of genes that responded to 20E or insulin at two time points. (B) Overlap between the hormone-dependent responses at 4 h (left), 9 h (right) or when each hormone supports the most amount of proliferation (bottom; 4 h for insulin, 9 h for 20E).

Unlike in the insulin targets, significantly enriched GO terms in the 20E-induced genes also describe a variety of developmental processes (Fig. 4). Genes with these GO terms include components and targets of the Notch, Wg, EGF and JAK/STAT pathways (Fig. 5). Also significantly affected was *sugarless*, which is required to synthesize the heparan sulfate moieties of proteoglycans needed for Dpp, Hh, FGF and Wg signaling (Hacker et al., 1997; Bornemann et al., 2004; Yan and Lin, 2009). 20E, and not insulin, also supports the expression of a wide variety of developmentally important transcription factors, chromatin-modifying proteins, and many genes that regulate tissue morphogenesis, including junctional, cytoskeletal and ECM components (Fig. 5). A smaller set of developmentally important genes seems to be regulated by either hormone; however, 20E generally causes a more potent and long-lasting response in this group (Fig. S6). Of the genes that only 20E induces, roughly 30% are already known to perturb wing development when mutated.

Although the expression of many of these patterning genes is stably maintained by 20E in culture, a subset of 20E genes are only normalized in culture after 9 h but less well at 4 h (Fig. 4B). This subset is enriched for genes involved in DNA replication, consistent with the higher proliferation index at 9 h than at 4 h in culture with 20E (Fig. 1Aiii,Biii). The molecular mechanisms responsible for this delay in full response remain unclear. We also identified 102 genes that were only responsive to 20E at 4 h and not 9 h, but only one GO term, cuticle production, was enriched in this subset (data not shown).

On the whole, these transcriptional data suggest that insulin transiently promotes proliferation through its well-understood effects on anabolic metabolism. 20E promotes proliferation over a longer time scale, but influences only a subset of the direct growth-promoting genes activated by insulin. Instead, 20E supports the expression of genes involved in wing patterning and morphogenesis.

Perturbation of 20E signaling disrupts wing disc patterning *in vivo*

To determine whether our transcriptomic data from explants reflect an *in vivo* requirement for 20E in maintaining patterning systems during growth, we genetically perturbed 20E signaling *in vivo* by transiently overexpressing a dominant-negative Ecdysone receptor (EcR-DN) during the third instar and then assessing its effect on a broad range of morphogen and PCP pathways (Fig. 6). EcR-DN expression autonomously reduces tissue size and mitotic cell number (Fig. S7A) (Herboso et al., 2015). However, the tissue appears otherwise healthy: apoptosis is not affected (Herboso et al., 2015; data not shown), and neither the localization nor protein levels of Discs large is perturbed (Fig. 6A).

Expressing EcR-DN in the dorsal compartment decreases Wg expression, both in the hinge and in the stripe at the DV boundary (Fig. 6Bi). The autonomous effect of EcR-DN on the DV boundary Wg stripe is more obvious when it is overexpressed in the posterior compartment (Fig. S8). In addition, wing discs deprived of 20E *in vivo* have severely reduced levels of Wg and also grow less (Fig. S9A, Fig. S7B). These results are consistent with previously published data using similar perturbations (Mirth et al., 2009; Herboso et al., 2015).

In wild-type discs, both E-Cadherin (Shotgun) and Delta are upregulated by Wg signaling on either side of the DV boundary (Micchelli et al., 1997; Jaiswal et al., 2006; de Celis and Bray, 1997). Dorsal EcR-DN expression prevents both from accumulating on the dorsal side of the DV boundary, consistent with reduced Wg signaling in this region (Fig. 6Bii,Biii). Like at the DV boundary, EcR-DN expression also affects elevated Delta expression on either side of a region of high Hedgehog signaling near the AP boundary (Fig. 6Bii). This effect on Delta is consistent with our transcriptomic data showing that mRNA levels of *Delta* itself, as well as those of effectors of the EGF and Notch pathways that regulate the AP Delta pattern, drop in culture without 20E (Fig. 5).

Also consistent with our transcriptomic data, we found that Dally-like protein levels are considerably reduced in the EcR-DN-expressing compartment (Fig. 6Biv). Given the broad effects of heparan sulfate proteoglycans on morphogen signaling, we therefore also looked at Hh and Dpp pathways. Indeed, EcR-DN decreases levels of pMad (a readout of Dpp signaling) in the posterior compartment (Fig. 6Ci). Furthermore, Hh protein levels and signaling are strongly affected (Fig. 6Cii-Civ). Hh staining intensity decreases in the posterior producing cells, consistent with roles for Dally and Dally-like in controlling its trafficking there (Eugster et al., 2007; Ayers et al., 2010, 2012). Furthermore, the gradient in the anterior receiving cells is diminished and the amplitude and range of Hedgehog signaling outputs are reduced. Ci is stabilized over a shorter distance from the AP boundary (Fig. 6Ciii). Engrailed expression is also reduced, both anterior to the AP boundary, where expression is activated by Hh signaling, and posteriorly where its expression is maintained independently of Hh by chromatin modifications (DeVido et al., 2008) (Fig. 6Civ). The Hh gradient and signaling output were severely reduced in wing discs from larvae deprived of 20E *in vivo*, confirming that the effects of EcR-DN expression reflect a real requirement for 20E (Fig. S9).

Development (2017) 144, 4406-4421 doi:10.1242/dev.155069

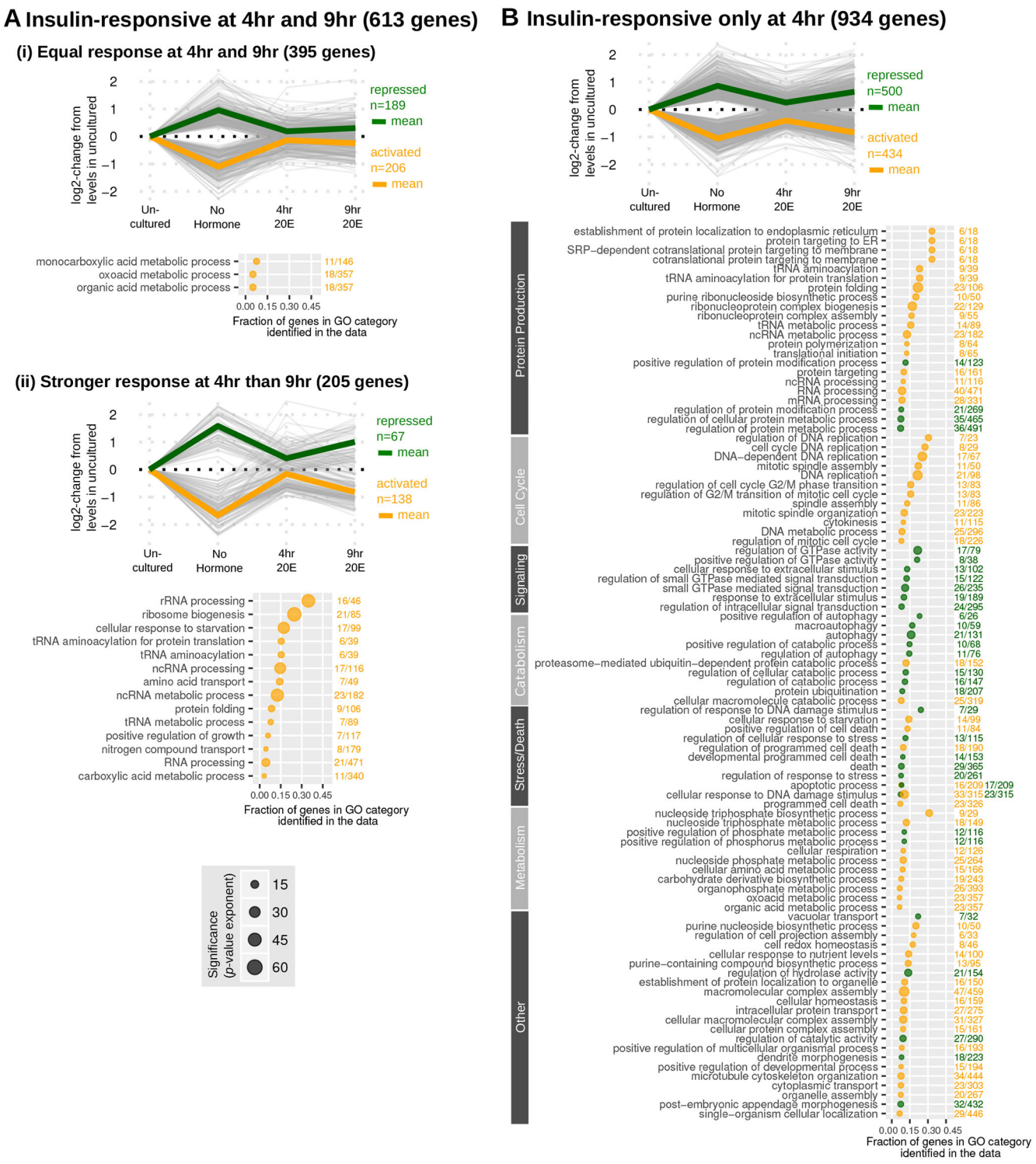

Fig. 3. Insulin-dependent gene expression in cultured wing discs. Genes were identified as responding to insulin at both time points (4 h and 9 h; A) or only at 4 h (B). Those in A were further subdivided into genes that are not significantly different between 4 h and 9 h (i), and genes that have a stronger response at 4 h than at 9 h (ii). For all genes of a subgroup, the fold change (log_2) in its expression from uncultured discs (96 h AEL) is shown in the top graph. Thick lines are the mean expression profiles for all genes that are repressed (green) or activated (orange). Below are the biological process GO terms that are significantly enriched in this subgroup, color-coded by whether the group is repressed (green) or activated (orange) and plotted by the fraction of its total genes that were identified in the data (number of genes in the data with this GO term/total size of the GO term; numbers reported to the right of the graph). The size of the circle indicates the significance of enrichment (exponent of the Benjamini–Hochberg-corrected *P*-value).

Our transcriptomic analysis also revealed that 20E affects the expression of the Core PCP component Prickle and the Fat PCP component Four-jointed (Fig. 5, Fig. S6). To examine global patterns of PCP, we stained for Dachsous (Ds) and Flamingo (Fmi; Starry night, Stan), which were not transcriptionally affected by 20E in culture but should nonetheless reveal any defects in the global patterns of PCP.

Development (2017) 144, 4406-4421 doi:10.1242/dev.155069

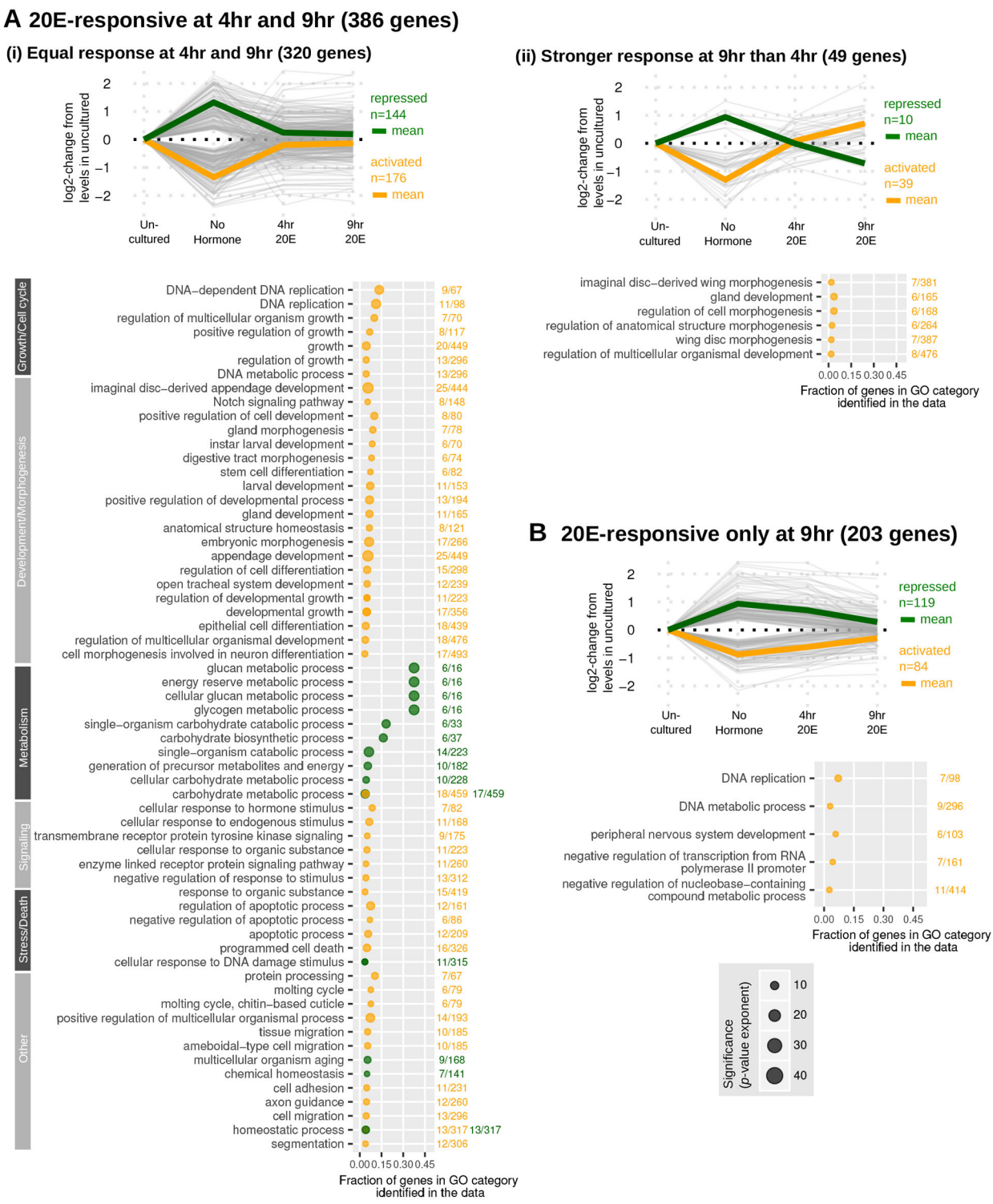

Fig. 4. 20E-dependent gene expression in cultured wing discs. Genes were identified as responding to 20E at both time points (4 h and 9 h; A) or only at 9 h (B). Those in A were further subdivided into genes that are not significantly different between 4 h and 9 h (i), and genes that have a stronger response at 9 h than at 4 h (ii). For all genes of a subgroup, the fold change (log_2) in its expression from uncultured discs (96 h AEL) is shown in the top graph. Thick lines are the mean expression profiles for all genes that are repressed (green) or activated (orange). Below are the biological process GO terms that are significantly enriched in this subgroup, color-coded by whether the group is repressed (green) or activated (orange) and plotted by the fraction of its total genes that were identified in the data (number of genes in the data with this GO term/total size of the GO term; numbers reported to the right of the graph). The size of the circle indicates the significance of enrichment (exponent of the Benjamini–Hochberg-corrected *P*-value).

Interestingly, EcR-DN expression was found to dramatically lower expression of both Ds and Fmi, presumably post-transcriptionally, such that any residual planar polarity was unquantifiable (Fig. 6D).

In summary, both *in vivo* experiments and transcriptomic data from explanted discs suggest that 20E is required to maintain the signal transduction and PCP pathways that drive growth and

Development (2017) 144, 4406-4421 doi:10.1242/dev.155069

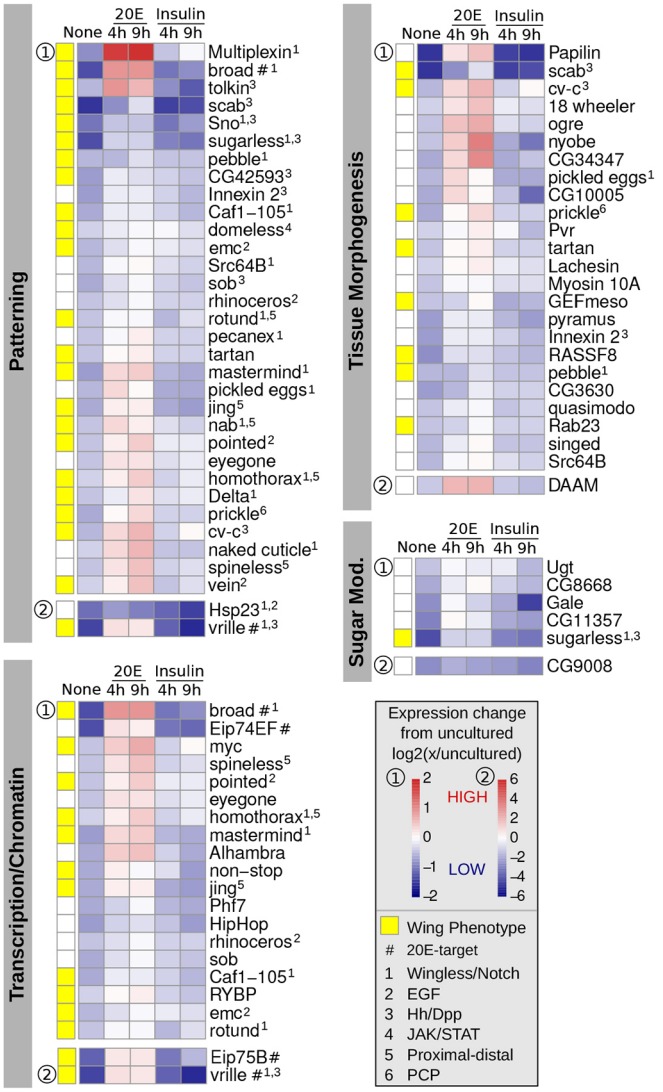

Fig. 5. Patterning and morphogenesis genes that are regulated by 20E in culture. Changes in the expression of selected 20E-regulated genes during wing disc culture (relative to their levels in uncultured, 96 h AEL discs) are shown for all conditions. Genes are plotted on one of two scales (labeled as 1 or 2), depending on the magnitude of their response. Yellow squares indicate genes with published loss-of-function phenotypes in the wing. Previously identified 20E-targets and genes with known connections to specific patterning systems (in any context) are indicated by superscript numbers. Mod., modification.

patterning in the wing disc. Given its key role in regulating patterning *in vivo* and *in vitro*, addition of 20E to explant culture could be crucial for measuring the normal patterning of growth.

Cellular contributions to oriented tissue growth

Having established that 20E supports longer proliferation and is better than insulin at maintaining the gene expression patterns underlying oriented growth, we used the new 20E-containing media to investigate the cell dynamics underlying growth and its anisotropy with live imaging. We analyzed the central wing pouch (shown in Fig. S10) of three discs in 13 h time-lapse experiments (shown together in Movie 1).

We first examined area change in the wing pouch and its cellular contributions (Fig. 7Bi). We note that tissue area (Fig. 7Bi, blue line) decreases during the first 2 h, almost entirely as a consequence of cell area changes (Fig. 7Bi, green line), suggesting that some time is required for discs to adapt to culture or recover from mounting. However, after the adaptation phase, tissue area grows. Cell divisions (Fig. 7Bi, orange line) contribute positively to tissue area growth and are only partly counteracted by modest levels of cell extrusion (Fig. 7Bi, cyan line) and slight cell area reduction (Fig. 7Bi, green line). This slight reduction in cell area is consistent with *in vivo* observations of growth over development time (Aegerter-Wilmsen et al., 2012; Mao et al., 2013).

To analyze the anisotropy of tissue growth in 20E, we measured the patterns of average pure tissue shear and its cellular contributions accumulated over 11 h after the 2 h adaptation phase using the Tissue Miner computational framework (Etournay et al., 2016) and Triangle Method (Merkel et al., 2017) (Fig. 7A, Fig. S11). Pure shear describes a change in aspect ratio that is independent of area change. In Fig. 7A, total tissue shear, determined on a grid of squares and accumulated over time, is indicated by lines, the length of which is proportional to the magnitude of pure shear and the orientation indicates its axis. We observe that tissue shear is oriented perpendicular to an axis defined by the DV boundary throughout the tracked region of the wing pouch, generally consistent with analyses of *in vivo* clone data (González-Gaitán et al., 1994; Resino et al., 2002; Baena-López et al., 2005; Worley et al., 2013; Mao et al., 2013; Heemskerk et al., 2014).

To examine the dynamics of tissue shape change, and its underlying cellular contributions, we calculated the average tissue shear and its cellular contributions over the entire tracked region using a coordinate system whose *x*-axis corresponding to the DV boundary (Fig. 7A, dotted horizontal line) and the *y*-axis perpendicular to it. In this coordinate system, a positive *xx* component of shear corresponds to shear parallel to the DV boundary, whereas a negative *xx* component of shear corresponds to shear perpendicular to the DV boundary. Fig. 7Bii (blue line) shows the *xx* component of the average tissue shear throughout the tracked region, accumulated over time. These plots reveal that the wing pouch becomes more anisotropic as it grows. Examining the cellular contributions to tissue shear reveals that cell divisions (Fig. 7Bii, orange line; see also Fig. S11) contribute to the change in shape of the wing pouch during growth. However, cell division orientation cannot entirely account for tissue shear: quantitatively similar contributions to tissue shear stem from both cell rearrangements (Fig. 7Bii, red line; see also Fig. S11) and cell shape changes (Fig. 7Bii, green line; see also Fig. S11).

Comparing the outlines of the wing pouch at the beginning and end of the movies (Fig. 7A) suggests that wing pouch tissue is expanding in a direction almost entirely perpendicular to the DV boundary. To quantify expansion along the *x*- and *y*-axes separately over time, we determined the *xx* and *yy* components of velocity gradient tensor based on the measured shear and area expansion (see supplementary Materials and Methods). Indeed, tissue expansion (Fig. 7Biii,Biv, blue lines) occurs along the *y*-axis, perpendicular to the DV boundary (Fig. 7Biv) and not along the *x*-axis (Fig. 7Biii). We decomposed the *xx* and *yy* components of the tissue velocity gradient tensor into their respective cellular contributions (see supplementary Materials and Methods). This calculation reveals that expansion of the wing pouch along the *y*-axis is almost identical to the expansion contributed by cell divisions in all three movies (compare orange and blue lines in Fig. 7Biv). Surprisingly, along the *x*-axis, the relationship between tissue flow and cell divisions is very different. Expansion due to cell divisions is only slightly smaller along the *x*-axis than along the *y*-axis (Fig. 7Biii,Biv, orange lines). Nevertheless, the *xx* component of tissue velocity gradient is small and negative, i.e. the tissue does not expand in this axis but

Development (2017) 144, 4406-4421 doi:10.1242/dev.155069

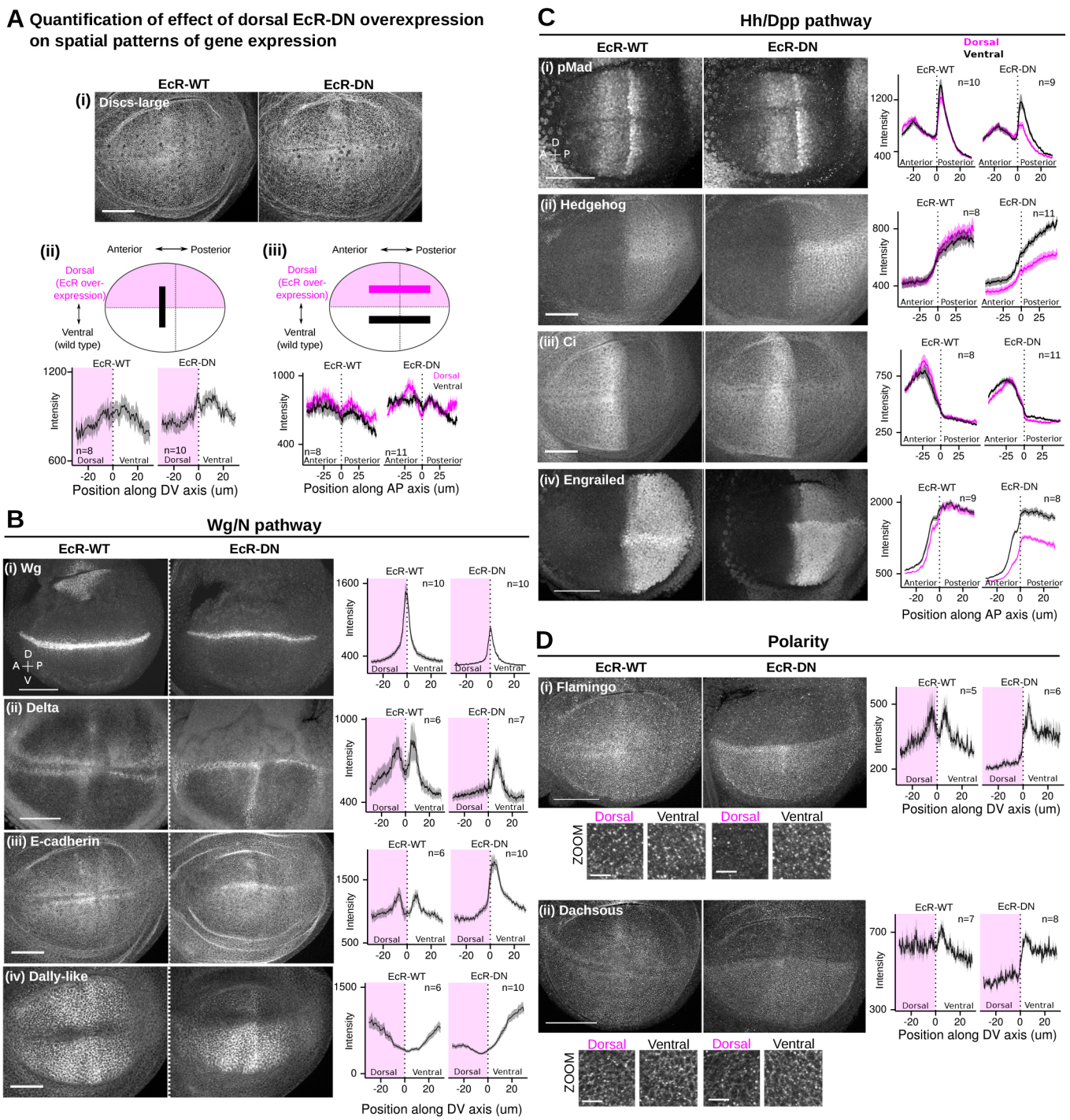

Fig. 6. Widespread effects on morphogen signaling and PCP upon perturbation of 20E signaling *in vivo*. (A-D) A dominant-negative allele of EcR-B1 (W650A, abbreviated EcR-DN) was overexpressed for 24 h in the dorsal compartment of the wing pouch (pink in the schematics in Aii,Aiii) using *apterous-GAL4* combined with temperature-sensitive *GAL80*. As a negative control performed in parallel, we overexpressed the wild-type EcR-B1 (EcR-WT), which does not significantly affect growth or proliferation of the disc (Fig. S7). Quantification of the expression patterns in this experiment was performed in one of two ways, each demonstrated in A for Discs-large (i), a septate junction marker. The first scheme (Aii) was used for proteins of the Wg/N (B) and PCP (D) pathways: the intensity profile (arbitrary units) along a line in the anterior compartment, drawn from dorsal (pink shaded) to ventral, was compared between EcR-WT- and EcR-DN-expressing discs. The second scheme (Aiii) was used for the Hh/Dpp pathways (C): the profile of absolute intensity along a line drawn from anterior to posterior in the dorsal compartment (pink) was compared with that along a line drawn in the ventral compartment (black). The lower images of Di and Dii are magnified regions from the anterior compartment of the images above. In all quantified intensity profiles, the solid line represents the mean of several discs from the same experiment (*n* noted on each graph), and the shaded ribbon is the s.d. Scale bars: 20 µm (D, zoom); 50 µm (all others).

rather contracts slightly. In this direction, the sum of the other cellular contributions is larger than along the *y*-axis and balances the contribution from cell divisions. We note that, although the contributions of cell shape changes, rearrangements and extrusions vary in each of the three movies, they always combine to cancel the expansion along the *x*-axis due to cell division.

Development (2017) 144, 4406-4421 doi:10.1242/dev.155069

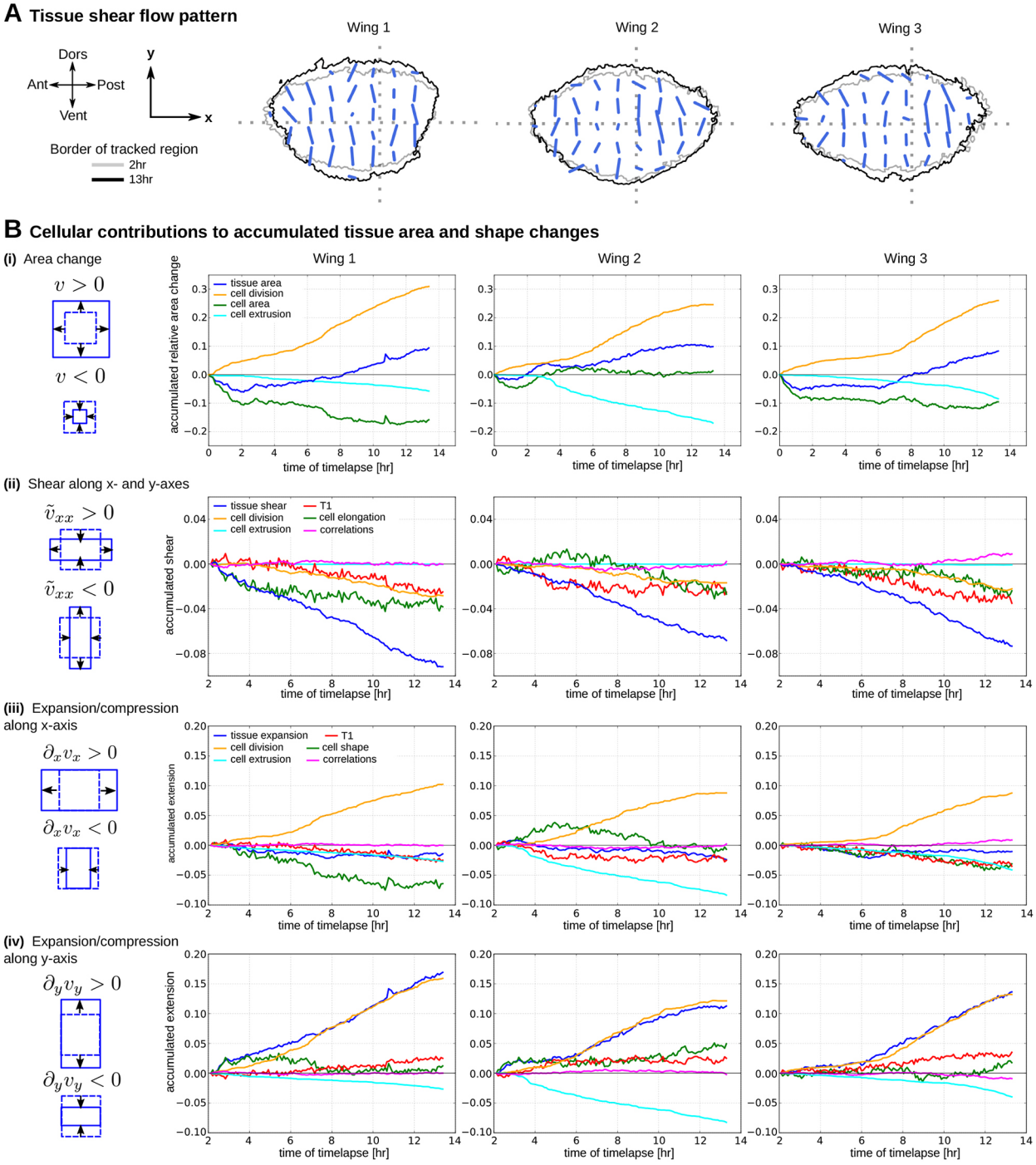

Fig. 7. Quantification of tissue growth and its cellular contributions. Three E-Cadherin-GFP-expressing wing discs were imaged for >13 h, and cells in the central pouch (future wing blade) were segmented and tracked. (A) Average tissue shear was accumulated between 2 h and 13 h in local regions of the tissue defined by a fixed grid with element size of 72 pixels (~14 µm). Shear patterns are plotted on outlines of the tracked region at 2 h (gray) and 13 h (black). (B) The trace of the velocity gradient tensor $v=\partial_x v_x+\partial_y v_y$ quantifies the relative change of tissue area. The diagonal component of the traceless symmetric part of the velocity gradient tensor $\tilde{v}_{xx} = \frac{\partial_x v_x - \partial_y v_y}{2}$ quantifies the tissue shear flow along *x*- and *y*-axes. (Bi) Relative change of tissue area, accumulated from the start of the time-lapse imaging, contains contributions from average cell area change, cell divisions and cell extrusions. (Bii) Accumulated tissue shear along the *x*-axis, averaged over the entire tracked region is plotted as a function of time (blue). The continuous shear of the blade perpendicular to the *x*-axis (negative values of blue curve) is composed of similar contributions from cell elongation change (green), T1 transitions (red) and cell divisions (orange). (Biii,Biv) Velocity gradient components $\partial_x v_x$ and $\partial_y v_y$ represent tissue extension or compression along the *x*- and *y*-axes, respectively. We calculated the accumulated extensions along *x*- and *y*-axes from the relative area change of the tissue and the tissue shear, and then calculated the cellular contributions to this deformation.

To confirm that cell elongation contributes to oriented growth *in vivo*, we quantified cell elongation in the wing pouch of explanted discs at 96 h, 119 h and 136 h AEL (Fig. 8). Indeed, the *xx* component of cell elongation becomes more negative over developmental time. This result is consistent with previously published patterns of cell elongation (Mao et al., 2013).

Development (2017) 144, 4406-4421 doi:10.1242/dev.155069

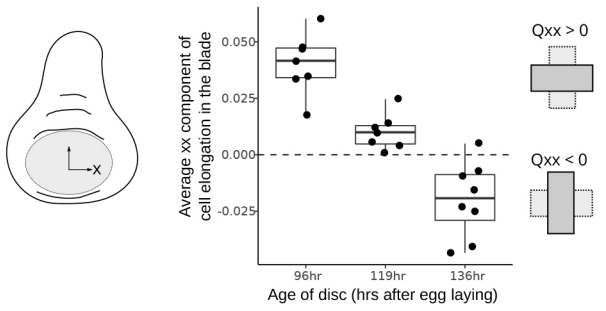

Fig. 8. Cell shapes in the wing pouch change over developmental time. E-cadherin-GFP-expressing wing discs were imaged live at three developmental time points. We designated an *x*-axis parallel to the DV boundary and calculated the *xx* component of cell elongation, averaged throughout the pouch (shaded region on the diagram). Positive values correspond to cells elongated parallel to the DV boundary, whereas negative values correspond to cells elongated perpendicular to it. Each dot represents the average value for one disc, and box plots summarize the data for each timepoint.

In summary, we use an improved method for long-term cultivation of wing imaginal discs to measure directly the cellular contributions to tissue shape and area changes. This analysis revealed that contributions from cell divisions to tissue shape changes are not nearly as anisotropic as tissue expansion and indicates that additional morphogenetic mechanisms exist to prevent expansion of the wing parallel to the DV boundary.

DISCUSSION

This work considerably expands our understanding of the cell dynamics in the growing *Drosophila* wing disc, revealing important contributions from cell rearrangements and cell shape changes to oriented tissue growth. Our analysis provides the foundation for future experiments aimed at understanding how patterned gene expression and tissue mechanics regulate cellular behavior during tissue growth. Furthermore, our transcriptomic data from wing discs cultured in 20E or insulin provide a novel global view of the direct response of wing imaginal tissues to these hormones. These data have *in vivo* implications for the organismal coordination of growth and development and constitute a valuable resource for the planning of any type of experiment requiring wing disc culture.

20E supports normal growth of cultured wing discs, independently of insulin

Studying the cellular basis of tissue development requires prolonged, high time resolution imaging that is ideally entirely *in vivo*. However, the *Drosophila* wing grows during larval stages, when animals are mobile and feeding. Although completely *in vivo* methods for visualizing wing disc growth continue to improve (Heemskerk et al., 2014), the currently available frame rate is still far too low to study cell dynamics. Analyzing whether cell boundary exchanges that are noisy and dynamic have an orientation, for example, demands the integration of high time resolution data over as much time as possible. Explant culture is the only option, provided that the patterning systems that drive oriented growth can be maintained.

Although previous studies have used insulin to sustain discs long term in culture (Zartman et al., 2013; Handke et al., 2014; Mao et al., 2011, 2013; Legoff et al., 2013; Heller et al., 2016; Tsao et al., 2016; Strassburger et al., 2017), we show that the expression of numerous genes involved in patterning declines when discs are cultured without the steroid hormone 20E. 20E was previously thought to promote imaginal growth by repressing the expression of the translational inhibitor 4E-BP (Herboso et al., 2015); however, we show here that, in addition, 20E broadly affects many different signaling pathways, each one of which is crucial for growth. These data indicate that the inclusion of 20E in culture media is vitally important to the goal of replicating *in vivo* growth patterns. Although high concentrations of 20E promote eversion, lower concentrations promote growth in the absence of insulin. This condition actually supports proliferation for longer than insulin-containing media: up to ∼24 h in 20E, compared with only ∼7-10 h in insulin (Fig. 1) (Zartman et al., 2013; Handke et al., 2014; Tsao et al., 2016).

How does the growth of 20E-cultured discs compare with growth *in vivo*? Although discs can proliferate in culture for up to 24 h, they slow down sooner (after ∼13 h) if they are continuously imaged. Nonetheless, for the first 13 h of live imaging, our direct quantification of the tissue growth pattern agrees well with results of indirect methods for following growth *in vivo* (González-Gaitán et al., 1994; Resino et al., 2002; Baena-López et al., 2005; Mao et al., 2013; Worley et al., 2013; Heemskerk et al., 2014). We also confirm data from fixed tissues (Baena-López et al., 2005) showing that cell division orientation has a slight bias toward a direction perpendicular to the DV boundary, at least in central regions of the pouch (compare orange lines in Fig. 7Biii,Biv). We estimate that the overall cell doubling time in continuously imaged explanted discs is about three times longer than the estimated rate in well-fed animals (Garcia-Bellido and Merriam, 1971; Bryant and Levinson, 1985; González-Gaitán et al., 1994; Heemskerk et al., 2014). However, phototoxicity associated with continuous imaging seems to affect not just the duration but also the rate of proliferation: estimating the rate from the density of PH3-stained nuclei in discs that were not continuously imaged suggests a value that is closer to that of freshly explanted discs (Fig. 1).

Interestingly, *in vivo*, if animals are starved after the attainment of a critical weight, the release of insulin-like peptides from the brain is reduced (Géminard et al., 2009) and growth arrests in the larval – but not imaginal – tissues (Britton and Edgar, 1998; Cheng et al., 2011). The rate of imaginal proliferation during this so-called 'sparing' condition is ∼60% lower than in the well-fed state (Cheng et al., 2011). Thus, proliferation of explants given 20E but not insulin may be closer to this *in vivo* low-insulin state. Importantly, although the ablation of insulin-producing cells in the brain reduces the size of the emerging adult wings, these wings are nevertheless well-proportioned (Rulifson et al., 2002). Thus, the orientation of tissue growth and its underlying cell dynamics is likely to be preserved in discs cultured with 20E in the absence of insulin. Perhaps the slight but reproducible lag in the division rate at early times of 20E culture (Fig. 1Biii, Fig. 7Bi) reflects a transition phase when discs taken from well-fed animals must switch to an insulin-independent/20E-dependent mode of growth.

Implications for hormonal regulation of growth

The mechanism underlying the sparing of imaginal tissues is unknown. Sparing of the central nervous system involves a locally provided ligand that activates downstream signaling in the insulin pathway (Cheng et al., 2011). Our transcriptomic data provide no evidence that wing discs can produce their own insulin-like ligands or that they can fully activate insulin signaling in the absence of exogenous ligands. Nonetheless, wing discs in culture continue to proliferate in 20E, even when no insulin-like ligand is present. This finding raises the possibility that 20E is also sufficient to support their proliferation *in vivo* during starvation. Although 20E promotes imaginal growth, it inhibits that of larval tissues (Delanoue et al.,

Development (2017) 144, 4406-4421 doi:10.1242/dev.155069

2010), potentially explaining the opposite response to starvation of these two tissue types.

Under well-fed conditions, insulin signaling must be able to combine with 20E signaling to further increase imaginal disc growth, but this feature is not well-reproduced in culture (Fig. 1Biv) (Handke et al., 2014; Strassburger et al., 2017). *Drosophila* has seven insulin-like peptides that interact not only with the single receptor, but also with other proteins that modulate their activities (Honegger et al., 2008; Arquier et al., 2008; Okamoto et al., 2013). Perhaps specific insulin peptides or their binding proteins allow proper interfacing with 20E signaling to promote growth.

Cellular dynamics underlying oriented tissue growth in the wing disc

Although the mechanisms dictating cell division orientation in this tissue have been studied (Mao et al., 2011, 2013; Legoff et al., 2013), the extent to which the observed slight bias in cell division orientation could account for the orientation of tissue growth has remained unclear. The Triangle Method (Merkel et al., 2017; Etournay et al., 2015) for decomposing tissue shape changes into quantitative contributions from all types of cellular events provides a measurement tool to connect the cell and tissue scales. Our results reveal that the observed bias in cell division orientation in the central region of the disc is insufficient to explain the anisotropy of tissue growth. Whereas expansion of the tissue perpendicular to the DV axis is driven primarily by cell divisions, in the orthogonal direction, cell shape changes and T1 transitions fully cancel the contribution to expansion by cell divisions, such that the wing does not expand along an axis parallel to the DV boundary.

Previous efforts to quantify cell rearrangements have used live imaging of discs cultured in insulin and have concluded that they occur either with very low frequency (Gibson et al., 2006; Legoff et al., 2013), or with a significant frequency but no pattern or orientation at the tissue scale (Mao et al., 2013; Heller et al., 2016). In contrast, we see that the contribution of cell rearrangements to tissue growth is quantitatively similar to that of oriented cell division and helps restrict growth parallel to the DV boundary. This discrepancy could result from either the differing culture conditions (lack or presence of 20E) or the inherent difficulties in defining and counting cell rearrangements. A classic T1 transition (Weaire and Rivier, 1984) occurs when two pairs of cells exchange neighborships, i.e. the connecting bond between two cells shrinks as all cells come together to make a four-way vertex; then, a new bond is formed such that the two cells that were originally separated come into contact, whereas the two that were originally together stay separate. But sometimes the four-way vertex simply resolves back without changing the original neighborship, and sometimes the neighborship fluctuates back and forth several times. How and when do you count the rearrangement? The method that we use overcomes the problem of having to classify a 'true' T1 event based on observation time windows. It considers all changes in neighborship, regardless of the length of time they persist, and quantifies their accumulated contribution to tissue shape change. Thus, we are not simply quantifying the number and orientation of T1s but the tissue shape change that they cause. This approach could be key to our ability to detect and quantify the important contribution of cell rearrangements to oriented growth of the wing disc.

What mechanisms might allow cell rearrangements, cell shape changes and cell extrusions to cancel expansion due to cell division specifically in one direction? We propose that a mechanical constraint prevents wing pouch expansion parallel, but not perpendicular, to the DV boundary. In this case, area growth due to cell division would lead to anisotropic expansion with corresponding anisotropic stresses that could be associated with oriented cell shape changes and rearrangements. Consistent with this hypothesis, we observe that the sum of expansion due to rearrangements, shape changes and extrusions is more reproducible than their individual cellular contributions. Long-range anisotropic stresses could coordinate these cellular processes and account for their mutual dependence. A similar dependence between cellular contributions is observed in the pupal wing, where the constant tissue area is maintained by epithelial tension via extracellular matrix connections to the cuticle (Etournay et al., 2015). We do not yet know whether the larval wing disc is mechanically constrained. It will be interesting to explore whether the extracellular matrix has anisotropic properties or whether the folding pattern of the tissue influences growth orientation.

The fact that Fat PCP mutant wings are associated with less anisotropic clone shapes and more weakly oriented cell divisions (Baena-López et al., 2005; Mao et al., 2011) has led to the idea that Fat orients growth through its effect on cell division orientation. We find that shear due to cell divisions cannot fully account for the anisotropy of growth, however. This result suggests either that there are other orienting factors, or that Fat PCP has more profound effects on growth anisotropy than can be accounted for by cell division.

Overall, this work opens new avenues towards an understanding of wing morphogenesis that integrates different scales – from the larval hormonal networks to the morphogen-dependent patterns of cell dynamics from which tissue shape emerges.

MATERIALS AND METHODS

Flies

The culture experiments described in Fig. 1 and the transcriptomic analyses were performed using wild-type OregonR *Drosophila*. For live-imaging experiments, we used animals in which the endogenous E-Cadherin gene had been fused with GFP (Huang et al., 2009). To enable temperature-inducible GAL4-dependent gene expression, we combined the *apterous-GAL4* (Marois et al., 2006), *phantom-GAL4* (Ono et al., 2006) and *engrailed-GAL4* (DeVido et al., 2008) loci with the temperature-sensitive GAL4 repressor GAL80^{ts} driven by the tubulin promoter. UAS-EcR.B1 (BDSC 6469) and UAS-EcR.B1-DeltaC655.W650A (BDSC 6872) (Cherbas et al., 2003) were acquired from Bloomington Stock Center (Bloomington, Indiana, USA). The line used to induce RNAi against *neverland* was obtained from the group of R. Niwa (Yoshiyama et al., 2006). To visualize FoxO, we used the *dfoxo-v3-mCherry* knock-in line generated by genomic recombineering of the endogenous *foxo* (Kakanj et al., 2016).

Flies were grown on standard media containing cornmeal, molasses agar and yeast extract under a 12 h light/dark cycle at 25°C (except when gene expression was induced using the temperature-sensitive GAL80, described below).

For all disc culture experiments, we used wing discs from larvae at 96 h AEL. Flies were allowed to lay eggs on apple juice agar plates (supplemented with yeast paste) for 1-2 h at 25°C. Agar pieces containing ∼10-12 eggs each were placed into food vials and grown at 25°C. The middle of the egg collection window was considered to be 0 h AEL.

Wing disc culture

Culture media

Early experiments (data not shown) indicated that overall disc morphology was best preserved in Grace's Insect culture medium, compared with Schneider's or Shield's and Sang. Thus, Grace's was used for all experiments. Grace's medium (Sigma, G9771) was prepared without sodium bicarbonate but with the addition of 5 mM BisTris. The pH was adjusted to 6.6-6.7 at room temperature, and the prepared liquid media was stored at 4°C for no longer than one month. On the day of the experiment, we added 5% fetal bovine serum (FBS; ThermoFisher/Invitrogen, 10270098)

Development (2017) 144, 4406-4421 doi:10.1242/dev.155069

and Penicillin-Streptomycin (Sigma P4333, 100× stock solution) to impede microbial growth. Note that although other groups have included female fly extract in the media (Zartman et al., 2013; Handke et al., 2014; Tsao et al., 2016), we found it to be less reproducible than FBS (data not shown). Furthermore, recent evidence indicates that fly extract is associated with non-physiological calcium waves in explanted wing discs (Balaji et al., 2017).

Stock solutions of either 20E or insulin were added just prior to the start of the experiment. 20E (Sigma, H5142) was added as a 1:1000 dilution from an ethanol stock solution (stored at −20°C, prepared fresh weekly) to give a final concentration of 20 nM in the media (except when otherwise noted). Bovine insulin (Sigma, I5500) was prepared as a 10 mg/ml stock solution in acidified water (stored at −20°C) and added at a final concentration of 5 µg/ml. This concentration of insulin is comparable to the levels used in previous studies aimed at prolonging proliferation of discs in culture (Zartman et al., 2013; Handke et al., 2014). Given that our data on the proliferation index in discs cultured in insulin alone (Fig. 1Bii) quantitatively agree with the results of these previous studies, the other differences between our culture media and theirs do not seem to be as important as hormonal content.

Culture procedure

To prepare larvae for dissection, we first floated them out of the food by adding 30% sucrose. Larvae were transferred using a brush or wide-tip transfer pipette into glass dishes. Excess food was removed by washing in sucrose, followed by distilled water. They were then surface sterilized by immersion in 70% ethanol for 1-2 min. Finally, they were washed once more with sterile water and then media. Except for the live-imaging experiments, discs were dissected in hormone-free media and then immediately transferred from the dissecting well into media containing hormone. For each experiment, dissections were performed over a period of no more than 45 min, and the start time of the culture was considered to be the midpoint of that dissection window. The number of discs analyzed per sample was limited by how many could be manually dissected as carefully as possible during that time window.

Discs were cultured in glass wells (Electron Microscopy Sciences; 70543-30) in 500 µl of growth media, with 10-20 discs per well, at 25°C in humidified chambers. Media was exchanged approximately every 2 h, except during the long incubations of 16-24 h, when there was a maximum incubation without media change of 8 h. At the end of culture, discs were fixed by exchanging the media with 4% paraformaldehyde (PFA; 8% PFA stock solution in PBS diluted into Grace's media). Discs were incubated for 20 min at room temperature and stained as described below in the immunofluorescence section.

The data presented in Fig. 1 represent a compilation of results from multiple days (labeled in different colors). Two replicates were carried out for each hormonal condition and time point. All discs were included in the analysis, except in rare cases when a disc was distorted during mounting.

Transcriptomic analysis

Sample preparation

Three biological replicates were performed for each hormone condition and time point. For each, ∼20-30 discs were dissected and cultured as described above and then transferred to a microfuge tube in a volume of 15-20 µl (growth media). Discs were frozen immediately in liquid nitrogen and stored at −80°C until all samples were ready for RNA isolation. A Qiagen RNeasy Mini kit was used to isolate RNA for sequencing. Samples were lysed by adding Buffer RLT+2-mercaptoethanol and vortexing for 20-30 s on ice. The manufacturer's instructions were followed for the rest of the protocol. Further purification was achieved with an ethanol precipitation.

Sequencing

mRNA was isolated from 1 µg total RNA by poly-dT enrichment using the NEBNext Poly(A) mRNA Magnetic Isolation Module according to the manufacturer's instructions (New England Biolabs). Final elution was performed in 15 µl of 2× first strand cDNA synthesis buffer. After chemical fragmentation by incubating for 15 min at 94°C, the sample was directly subjected to the workflow for strand-specific RNA-Seq library preparation (Ultra Directional RNA Library Prep, New England Biolabs). For ligation, custom adaptors were used (Adaptor-Oligo 1: 5′-ACACTCTTTCCCTAC-ACGACGCTCTTCCGATCT-3′, Adaptor-Oligo 2: 5′-P-GATCGGAAG-AGCACACGTCTGAACTCCAGTCAC-3′). After ligation, adapters were depleted with an XP bead purification (Beckman Coulter), adding beads in a ratio of 1:1. Indexing was carried out during the following PCR enrichment (15 cycles) using custom amplification primers carrying the index sequence indicated with 'NNNNNN' (primer 1: Oligo_Seq 5′-AATGATACGGCG-ACCACCGAGATCTACACTCTTTCCCTACACGACGCTCTTCCGATC-T-3′; primer 2: 5′-GTGACTGGAGTTCAGACGTGTGCTCTTCCGAT-CT-3′; primer 3: 5′-CAAGCAGAAGACGGCATACGAGATNNNNNN-GTGACTGGAGTT-3′). After two more XP beads purifications (1:1), libraries were quantified using Qubit dsDNA HS Assay Kit (Invitrogen). Equimolar amounts of each sample were pooled and distributed amongst four lanes of an Illumina HiSeq 2500 sequencer for 75 bp single-end sequencing. On average we achieved 37 million reads per sample.

Processing of sequencing data

Short-read data was trimmed using Cutadapt (Martin, 2011) and aligned using TopHat2 (Kim et al., 2013). Differential gene expression analysis was performed for all pairwise comparisons between conditions and time points using Cufflinks (Trapnell et al., 2012). Our threshold for significance was $q<0.01$. We considered a gene to be expressed if it had a normalized count of fpkm (fragments per kilobase of transcript per million mapped reads)>5.

Raw sequencing data and fpkm normalized expression data files have been deposited in NCBI's Gene Expression Omnibus and are accessible through GEO Series accession number GSE92933.

Analysis of hormone-responsive gene sets

The identification of hormone-responsive gene sets was achieved by selectively filtering the differentially expressed genes table from Cufflinks using custom R scripts. First, we identified the genes in this table for which levels were significantly different ($q<0.01$) between no culture (freshly dissected discs from the beginning of the experiment, 96 h AEL) and culture without hormone (4 h). We split this culture-responsive subset into two groups based on whether their levels in uncultured discs were abnormally low or high after culture without hormone. To identify hormone-activated genes, we first identified the genes for which expression was abnormally low in culture with no hormone (relative to uncultured control). Amongst these, we identified genes whose levels were significantly elevated (either at 4 h or 9 h) when discs were cultured with hormone (compared with culture with no hormone). Hormone-repressed genes had the opposite pattern: abnormally high when cultured without hormone but significantly lower in culture with hormone. Additional information is provided in the supplementary Materials and Methods.

The Venn diagrams presented in Fig. 2 were generated using the VennDiagram package of R (Chen and Boutros, 2011) after identifying the genes that were unique or common in each pairwise comparison. We provide the gene lists that were used to create these graphs in Tables S1-S5. These lists also include information about whether the expression of each gene in culture without hormone is abnormally low or high, relative to its levels in uncultured discs.

We identified enriched Gene Ontology (GO) terms (Biological Process and Cellular Component) within each hormone-responsive dataset using the R-package ClusterProfiler (v 1.9) (Yu et al., 2012). To reduce redundancy, we used the simplify function of this package; similarity cutoff=0.95 and BH-corrected *P*-value cutoff=0.01. We also required enriched GO terms to have more than five genes included in the data. In Figs 3, 4 and Fig. S2, we only present the subcategories that have more than one enriched GO term.

For selected genes, we plotted the change in expression levels across all conditions (Fig. 5; Figs S2, S3, S6) using the pheatmap package in R. We took the $\log_2$ of the normalized counts (fpkm) in each condition divided by that in the uncultured wing discs (at 96 h AEL, time 0 h).

For the 589 genes regulated by 20E (either exclusively or also by insulin), we manually classified functional groupings after reviewing related literature, GO term assignments and FlyBase annotations. These groupings are described in the supplementary Materials and Methods.

In Figs S3 and S6, TOR targets were selected based on previous studies (Teleman et al., 2008; Guertin et al., 2006). The FoxO targets were selected

Development (2017) 144, 4406-4421 doi:10.1242/dev.155069

based on the experimental verifications in published studies (Puig et al., 2003; Teleman et al., 2008; Olson et al., 2013; Chen and Boutros, 2011; Lee et al., 2010). Most direct FoxO targets identified using adult females (Alic et al., 2011) were either not differentially expressed in our culture conditions or not insulin sensitive [i.e. Su(Hw), Akt1, Pi3K68D, Indy; data not shown]. Note, however, that FoxO target genes have been shown to be variable, depending on tissue and developmental stage (Teleman et al., 2008; Alic et al., 2011).

In Fig. 5, 20E targets were taken from previous publications (Beckstead et al., 2005; Gauhar et al., 2009).

Temperature-sensitive GAL4/GAL80^{ts} experiments

Apterous-GAL4, GAL80^{ts}/CyO-GFP females were crossed with males of *UAS-EcR* or *UAS-EcR-W650A*, and their progeny were kept at 18°C (permissive for GAL80 repressor function) on Bromophenol Blue-containing food for 7-8 days. Vials were then moved to 29°C (restrictive) to induce GAL4-dependent transcript of EcR constructs for 24 h. Upcrawling larvae were selected for dissection based on the absence of GFP and the presence of blue food in the gut (indicating that they are still many hours from pupariation) (Andres and Thummel, 1994).

To remove circulating 20E, *UAS-CD8-GFP;;phantom-GAL4, GAL80^{ts}/TM3-GFP* females were crossed with males of the *neverland* targeting line, and their progeny were kept at 18°C. Vials were shifted to 29°C, and discs from upcrawling larvae lacking the *TM3-GFP* balancer were dissected 2 or 4 days later. As controls, we used progeny of *UAS-CD8-GFP;;phantom-GAL4, GAL80^{ts}/TM3-GFP* females crossed to *w^{1118}* flies in parallel. The progeny of the control cross all pupariated by 2 days after the shift to 29°C.

Immunofluorescence

Primary antibodies used were: anti-Ci-full length [1:100, rat, Developmental Studies Hybridoma Bank (DSHB) 2A1 conc], anti-Dally-like (1:100, mouse, DSHB 13G8 conc), anti-Dachsous (1:1000, mouse; Merkel et al., 2014), anti-Delta (1:800, mouse, DSHB C594.9B, conc), anti-Engrailed (1:100, mouse, DSHB 4D9 conc), anti-Discs-large (1:100, mouse, DSHB 4F3), anti-E-Cadherin (1:100, rat, DSHB DCAD2 sup), anti-Flamingo (1:200, rabbit; Sagner et al., 2012), anti-Hh (1:500, rabbit; Eugster et al., 2007), anti-mCherry (1:500, ThermoFisher, PA5-34974), anti-Patched (1:100, mouse, DSHB Apa1 conc), anti-pHistoneH3-Ser10 (1:1000, rabbit, Cell Signaling, #9701), anti-pMAD (1:1000, rabbit, Epitomics, 1880-1), anti-Wg (1:100, mouse, DSHB 4D4).

Secondary antibodies used were: Alexa Fluor-488 goat anti-rabbit (1:1000, ThermoFisher, A11034), Alexa Fluor-555 goat anti-mouse (1:1000, ThermoFisher, A21424), Alexa Fluor-647 goat anti-rat (1:500, ThermoFisher, A21247).

Discs were dissected in PBS and then fixed and stained according to standard methods (detailed in the supplementary Materials and Methods).

Imaging of fixed samples was performed using an Olympus FV1000 laser-scanning confocal microscope fitted with an Olympus BX61 inverted stand and motorized *xyz* stage, driven by FV10-ASW 1.7 software. Wing discs were imaged using either an Olympus UApochromat 40×1.35NA oil immersion or an Olympus UPlanSApochromat 60×1.35NA oil immersion objective.

All discs were imaged and analyzed, except in very rare cases when the discs were damaged or misshapen during mounting.

Analysis of immunofluorescence images

Phospho-Histone H3

z-stacks of wing discs stained with PH3 were analyzed in 2D after a maximum intensity projection. PH3+ nuclei were segmented using Fiji Weka segmentation plugin (Arganda-Carreras et al., 2017). A training set containing images from each condition of the experiment was used to generate a common classifier, which was then applied to all images. Probability masks were thresholded by likelihood and size. The wing pouch was identified morphologically by the innermost folds in the epithelium. Compartment and wing pouch size in Fig. S7 was measured on a 2D projection, using Fiji to identify the region of interest manually (guided by E-cadherin or EcR staining). Plotting was performed in R. For all box plots, the hinges correspond to the first and third quartiles; lines indicate the highest and lowest values within 1.5*IQR (inter-quartile range); outlier points are black, except in Fig. S7Aiii, where they are blue.

Cell area in fixed samples

In Fig. 1C, apical cell areas were determined and plotted using Tissue Analyzer (Aigouy et al., 2016) to segment cells based on E-Cadherin staining, and Tissue Miner (Etournay et al., 2016) to determine the area and position of each cell.

Intensity profiles

The changes to patterns of protein production/localization upon *in vivo* perturbation of 20E signaling were analyzed in a 2D maximum intensity projection. Using Fiji (Schindelin et al., 2012), a line 50 pixels wide (~20 µm) was drawn either from dorsal to ventral in the anterior and posterior compartments or from anterior to posterior in the dorsal and ventral compartments. Absolute intensity values along these lines were averaged across all samples (imaged on the same day, under the same acquisition settings). Plotted is the mean and standard deviation of intensity along these lines. At least five discs were imaged per biological condition; exact numbers are shown in the figures.

Long-term time-lapse imaging

Discs were dissected directly in growth media containing hormone. For imaging, discs were gently immobilized under a porous filter (Whatman cyclopore polycarbonate membranes; Sigma, WHA70602513) in a 35 mm glass-bottomed Petri dish (Mattek, P35G-1.0-14-C) using double-sided adhesive tape (Tesa 5338, doppelband fotostrip, ~100 µm thick) as a spacer between the glass and the filter. To construct this chamber, we first punched a hole (6 mm) in the tape, and then adhered the tape to the glass. The discs were transferred in ~10 µl media to the center of the hole in the tape spacer. Care was taken to keep the tape dry. Discs were carefully arranged to be apical-side down (towards the coverslip) using forceps. Most of the media was then removed, and the filter (cut approximately to the size of the tape) was quickly placed over the sample and firmly adhered to the tape with forceps. The dish was then filled with 2-3 ml media. The height of these chambers is greater than the height of the discs, but the presence of the filter isolates the discs from flows and somewhat constrains disc movements so that they usually remain in the field of view. As an alternative, we also tried to immobilize discs using methylcellulose (Aldaz et al., 2010) dissolved in our culture medium, but discs are very hard to position in this media and often do not proliferate.

During imaging, we used a syringe pump (PHD ULTRA, Harvard Apparatus) to exchange the media automatically and continuously during the course of imaging at a rate of 0.03 ml/min. The start of the movie was considered to be time 0 h. This time corresponds to 45-60 min from the start of dissection (time required for sample preparation and microscope setup).

Imaging was performed using a Zeiss spinning-disc microscope consisting of an AxioObserver inverted stand, motorized *xyz* stage with temperature control set to 25°C, Yokogawa CSU-X1 scanhead, and a Zeiss AxioCam MRm camera (2×2 binning), all controlled by Axiovision software. Discs were imaged through a Zeiss C-Apochromat 63×1.2NA water immersion objective heated to 25°C with an objective heater. To capture the whole pouch, we acquired a 2×2 tiled region (10% overlap). Each region consisted of a *z*-stack of 65-85 frames, spaced 0.5 µm apart. Tiled *z*-stacks were captured every 5 min. We kept light exposure as low as possible to achieve a segmentable image. We used a power meter (PT9610, Gigahertz-optik, Munich, Germany) to measure the power of the laser through a 10×/0.45 NA objective within a week of the experiment. For imaging, we used a laser power of 0.04-0.05 mW and an exposure time of 350 ms per image.

Analysis of live imaging

Image processing, segmentation, and cell tracking

Raw data were first processed with a low-pass frequency filter to remove high-frequency noise, followed by a rolling-ball background-subtraction algorithm using Fiji (Schindelin et al., 2012). The apical plane was projected onto 2D using a custom-made algorithm. We identified the two manifolds formed by the disc proper layer and the peripodial layer, respectively, in the 3D *z*-stacks, based on maximal brightness of the E-Cadherin-GFP signal and subject to

Development (2017) 144, 4406-4421 doi:10.1242/dev.155069

hard constraints on the distance between the two layers and the slope of each manifold. We employed the algorithm of Wu and Chen (2002) to determine simultaneously the two manifolds that are optimal, i.e. as bright as possible under the given constraints. This algorithm and its application to the wing disc will be described in detail in a separate upcoming manuscript (details available upon request).

Projected tiles were stitched using the Grid/Collection Stitching Fiji plugin (Preibisch et al., 2009). Segmentation and cell tracking was performed on the projected images of the time lapse using Tissue Analyzer (Aigouy et al., 2016). We oriented the tissue to have the DV boundary as the horizontal *x*-axis using TissueMiner (Etournay et al., 2016).

Analysis of cellular contributions to changes in tissue size and shape

The analysis of tissue shear and its cellular contributions was performed on the region of the central wing pouch that was trackable throughout the entire course of our movies. The cells belonging to this region in the first frame of the time-lapse movie are visualized in Fig. S10. We defined this region using Tissue Miner (Etournay et al., 2016) by first manually marking the region between the two innermost folds of the pouch in the last frame of the time-lapse movie, and then backtracking these cells and their lineages to the first time point, discarding cells that moved in/out of the field of view.

Analysis of cellular contributions to changes in tissue size and shape were calculated using the Triangle Method (Merkel et al., 2017) and Tissue Miner (Etournay et al., 2016). Further details are provided in the supplementary Materials and Methods.

Analysis of cell shape over developmental time

For the plot shown in Fig. 8, we dissected wing discs from E-cadherin-GFP-expressing larvae at 96 h, 119 h and 135 h AEL. Note that the E-cadherin-GFP flies are slightly developmentally delayed, taking ∼135 h to pupariate, compared with ∼120 h for OregonR. Discs were mounted as for live imaging, in 20E-containing culture media, and imaged within 1 h of dissection. *z*-stacks were acquired, processed and projected, as described for live imaging. The cells belonging to the central pouch region (defined as the region between the two innermost folds) were manually identified and marked using TissueMiner (Etournay et al., 2016). This region should correspond roughly to the same regions analyzed in the movies presented in Fig. 7. Tissues were oriented so that the DV boundary would be the horizontal *x*-axis, as for live imaging. In Fig. 8, we plot for each disc the area-weighted average of triangle elongation in the identified region of analysis. The box plots in Fig. 8 summarize the data for each age group: hinges correspond to the first and third quartiles; lines indicate the highest and lowest values within 1.5*IQR (inter-quartile range).

Acknowledgements

RNA sequencing was performed by Annekathrin Kränkel and Andreas Dahl in the Deep Sequencing Group SFB655 at the Biotechnology Center of the Technische Universitaet Dresden. The processing of the RNAseq data was performed with considerable help from Holger Brandl of the Bioinformatics facility of the MPI-CBG. We thank Marko Brankatschk, Christian Dahmann, and Savraj Grewal for critical review of the manuscript prior to submission.

Competing interests

The authors declare no competing or financial interests.

Author contributions

Conceptualization: N.A.D., F.J., S.E.; Methodology: N.A.D., M.P., R.E., D.K., E.W.M., F.J.; Software: N.A.D., M.P., R.E., D.K.; Validation: N.A.D., S.S., S.G.; Formal analysis: N.A.D., M.P., R.E., F.J.; Investigation: N.A.D., M.P., S.S., S.G., F.J., S.E.; Resources: E.W.M., F.J., S.E.; Data curation: N.A.D., M.P.; Writing - original draft: N.A.D., M.P., F.J., S.E.; Writing - review & editing: N.A.D., M.P., S.S., R.E., F.J., S.E.; Visualization: N.A.D., M.P.; Supervision: E.W.M., F.J., S.E.; Project administration: F.J., S.E.; Funding acquisition: S.E.

Funding

Funding for this project was provided by a European Molecular Biology Organization Long Term Postdoc Fellowship (to N.A.D.), Marie Curie PostDoc fellowship from the EU Seventh Framework Programme (to R.E.), a grant from the Deutsche Forschungsgemeinschaft (SPP1782 to S.E.), and the Max-Planck-Gesellschaft and Bundesministerium für Bildung und Forschung.

Data availability

The sequencing data discussed in this publication have been deposited in NCBI's Gene Expression Omnibus and are accessible through GEO Series accession number GSE92933.

Supplementary information

Supplementary information available online at
http://dev.biologists.org/lookup/doi/10.1242/dev.155069.supplemental

References

Aegerter-Wilmsen, T., Heimlicher, M. B., Smith, A. C., De Reuille, P. B., Smith, R. S., Aegerter, C. M. and Basler, K. (2012). Integrating force-sensing and signaling pathways in a model for the regulation of wing imaginal disc size. *Development* **139**, 3221-3231.

Affolter, M. and Basler, K. (2007). The Decapentaplegic morphogen gradient: from pattern formation to growth regulation. *Nat. Rev. Genet.* **8**, 663-674.

Aigouy, B., Umetsu, D. and Eaton, S. (2016). Segmentation and quantitative analysis of epithelial tissues. *Methods Mol. Biol.* **1478**, 227-239.

Aldaz, S., Escudero, L. M. and Freeman, M. (2010). Live imaging of Drosophila imaginal disc development. *Proc. Natl. Acad. Sci. USA* **107**, 14217-14222.

Alic, N., Andrews, T. D., Giannakou, M. E., Papatheodorou, I., Slack, C., Hoddinott, M. P., Cocheme, H. M., Schuster, E. F., Thornton, J. M. and Partridge, L. (2011). Genome-wide dFOXO targets and topology of the transcriptomic response to stress and insulin signalling. *Mol. Syst. Biol.* **7**, 502.

Ambegaonkar, A. A., Pan, G., Mani, M., Feng, Y. and Irvine, K. D. (2012). Propagation of Dachsous-Fat planar cell polarity. *Curr. Biol.* **22**, 1302-1308.

Andres, A. J. and Thummel, C. S. (1994). Methods for quantitative analysis of transcription in larvae and prepupae. *Methods Cell Biol.* **44**, 565-573.

Arganda-Carreras, I., Kaynig, V., Rueden, C., Eliceiri, K. W., Schindelin, J., Cardona, A. and Sebastian Seung, H. (2017). Trainable Weka Segmentation: a machine learning tool for microscopy pixel classification. *Bioinformatics* **33**, 2424-2426.

Arquier, N., Géminard, C., Bourouis, M., Jarretou, G., Honegger, B., Paix, A. and Léopold, P. (2008). Drosophila ALS regulates growth and metabolism through functional interaction with insulin-like peptides. *Cell Metab.* **7**, 333-338.

Aw, W. Y. and Devenport, D. (2017). Planar cell polarity: global inputs establishing cellular asymmetry. *Curr. Opin. Cell Biol.* **44**, 110-116.

Ayers, K. L., Gallet, A., Staccini-Lavenant, L. and Thérond, P. P. (2010). The long-range activity of Hedgehog is regulated in the apical extracellular space by the glypican Dally and the hydrolase Notum. *Dev. Cell* **18**, 605-620.

Ayers, K. L., Mteirek, R., Cervantes, A., Lavenant-Staccini, L., Therond, P. P. and Gallet, A. (2012). Dally and Notum regulate the switch between low and high level Hedgehog pathway signalling. *Development* **139**, 3168-3179.

Baena-López, L. A., Baonza, A. and García-Bellido, A. (2005). The orientation of cell divisions determines the shape of Drosophila organs. *Curr. Biol.* **15**, 1640-1644.

Balaji, R., Bielmeier, C., Harz, H., Bates, J., Stadler, C., Hildebrand, A. and Classen, A.-K. (2017). Calcium spikes, waves and oscillations in a large, patterned epithelial tissue. *Sci. Rep.* **7**, 42786.

Beckstead, R. B., Lam, G. and Thummel, C. S. (2005). The genomic response to 20-hydroxyecdysone at the onset of Drosophila metamorphosis. *Genome Biol.* **6**, R99.

Beira, J. V. and Paro, R. (2016). The legacy of Drosophila imaginal discs. *Chromosoma* **125**, 573-592.

Bodenstein, D. (1943). Hormones and tissue competence in the development of Drosophila. *Biol. Bull.* **84**, 34-58.

Bornemann, D. J., Duncan, J. E., Staatz, W., Selleck, S. and Warrior, R. (2004). Abrogation of heparan sulfate synthesis in Drosophila disrupts the Wingless, Hedgehog and Decapentaplegic signaling pathways. *Development* **131**, 1927-1938.

Brennan, C. A., Ashburner, M. and Moses, K. (1998). Ecdysone pathway is required for furrow progression in the developing Drosophila eye. *Development* **125**, 2653-2664.

Brennan, C. A., Li, T. R., Bender, M., Hsiung, F. and Moses, K. (2001). Broad-complex, but not ecdysone receptor, is required for progression of the morphogenetic furrow in the Drosophila eye. *Development* **128**, 1-11.

Brittle, A., Thomas, C. and Strutt, D. (2012). Planar polarity specification through asymmetric subcellular localization of Fat and Dachsous. *Curr. Biol.* **22**, 907-914.

Britton, J. S. and Edgar, B. A. (1998). Environmental control of the cell cycle in Drosophila: nutrition activates mitotic and endoreplicative cells by distinct mechanisms. *Development* **125**, 2149-2158.

Bryant, P. J. and Levinson, P. (1985). Intrinsic growth control in the imaginal primordia of Drosophila, and the autonomous action of a lethal mutation causing overgrowth. *Dev. Biol.* **107**, 355-363.

Bryant, P. J., Huettner, B., Held, L. I., Jr, Ryerse, J. and Szidonya, J. (1988). Mutations at the fat locus interfere with cell proliferation control and epithelial morphogenesis in Drosophila. *Dev. Biol.* **129**, 541-554.

Chen, H. and Boutros, P. C. (2011). VennDiagram: a package for the generation of highly-customizable Venn and Euler diagrams in R. *BMC Bioinformatics* **12**, 35.
Cheng, L. Y., Bailey, A. P., Leevers, S. J., Ragan, T. J., Driscoll, P. C. and Gould, A. P. (2011). Anaplastic lymphoma kinase spares organ growth during nutrient restriction in Drosophila. *Cell* **146**, 435-447.
Cherbas, L., Hu, X., Zhimulev, I., Belyaeva, E. and Cherbas, P. (2003). EcR isoforms in Drosophila: testing tissue-specific requirements by targeted blockade and rescue. *Development* **130**, 271-284.
Clark, H. F., Brentrup, D., Schneitz, K., Bieber, A., Goodman, C. and Noll, M. (1995). Dachsous encodes a member of the cadherin superfamily that controls imaginal disc morphogenesis in Drosophila. *Genes Dev.* **9**, 1530-1542.
De Celis, J. F. and Bray, S. (1997). Feed-back mechanisms affecting Notch activation at the dorsoventral boundary in the Drosophila wing. *Development* **124**, 3241-3251.
Delanoue, R., Slaidina, M. and Léopold, P. (2010). The steroid hormone ecdysone controls systemic growth by repressing dMyc function in Drosophila fat cells. *Dev. Cell* **18**, 1012-1021.
Devido, S. K., Kwon, D., Brown, J. L. and Kassis, J. A. (2008). The role of Polycomb-group response elements in regulation of engrailed transcription in Drosophila. *Development* **135**, 669-676.
Etournay, R., Popović, M., Merkel, M., Nandi, A., Blasse, C., Aigouy, B., Brandl, H., Myers, G., Salbreux, G., Jülicher, F. et al. (2015). Interplay of cell dynamics and epithelial tension during morphogenesis of the Drosophila pupal wing. *Elife* **4**, e07090.
Etournay, R., Merkel, M., Popovic, M., Brandl, H., Dye, N. A., Aigouy, B., Salbreux, G., Eaton, S. and Julicher, F. (2016). TissueMiner: a multiscale analysis toolkit to quantify how cellular processes create tissue dynamics. *Elife* **5**, e14334.
Eugster, C., Panáková, D., Mahmoud, A. and Eaton, S. (2007). Lipoprotein-heparan sulfate interactions in the Hh pathway. *Dev. Cell* **13**, 57-71.
Fristrom, J. W., Logan, W. R. and Murphy, C. (1973). The synthetic and minimal culture requirements for evagination of imaginal discs of Drosophila melanogaster in vitro. *Dev. Biol.* **33**, 441-456.
Garcia-Bellido, A. and Merriam, J. R. (1971). Parameters of the wing imaginal disc development of Drosophila melanogaster. *Dev. Biol.* **24**, 61-87.
Gauhar, Z., Sun, L. V., Hua, S., Mason, C. E., Fuchs, F., Li, T.-R., Boutros, M. and White, K. P. (2009). Genomic mapping of binding regions for the Ecdysone receptor protein complex. *Genome Res.* **19**, 1006-1013.
Géminard, C., Rulifson, E. J. and Léopold, P. (2009). Remote control of insulin secretion by fat cells in Drosophila. *Cell Metab.* **10**, 199-207.
Gershman, B., Puig, O., Hang, L., Peitzsch, R. M., Tatar, M. and Garofalo, R. S. (2007). High-resolution dynamics of the transcriptional response to nutrition in Drosophila: a key role for dFOXO. *Physiol. Genomics* **29**, 24-34.
Gibson, M. C., Patel, A. B., Nagpal, R. and Perrimon, N. (2006). The emergence of geometric order in proliferating metazoan epithelia. *Nature* **442**, 1038-1041.
González-Gaitán, M., Capdevila, M. P. and García-Bellido, A. (1994). Cell proliferation patterns in the wing imaginal disc of Drosophila. *Mech. Dev.* **46**, 183-200.
Guertin, D. A., Guntur, K. V. P., Bell, G. W., Thoreen, C. C. and Sabatini, D. M. (2006). Functional Genomics identifies TOR-regulated genes that control growth and division. *Curr. Biol.* **16**, 958-970.
Guirao, B., Rigaud, S. U., Bosveld, F., Bailles, A., Lopez-Gay, J., Ishihara, S., Sugimura, K., Graner, F. and Bellaiche, Y. (2015). Unified quantitative characterization of epithelial tissue development. *Elife* **4**, e08519.
Hacker, U., Lin, X. and Perrimon, N. (1997). The Drosophila sugarless gene modulates Wingless signaling and encodes an enzyme involved in polysaccharide biosynthesis. *Development* **124**, 3565-3573.
Handke, B., Szabad, J., Lidsky, P. V., Hafen, E. and Lehner, C. F. (2014). Towards long term cultivation of Drosophila wing imaginal discs in vitro. *PLoS ONE* **9**, e107333.
Hartl, T. A. and Scott, M. P. (2014). Wing tips: The wing disc as a platform for studying Hedgehog signaling. *Methods* **68**, 199-206.
Heemskerk, I., Lecuit, T. and Legoff, L. (2014). Dynamic clonal analysis based on chronic in vivo imaging allows multiscale quantification of growth in the Drosophila wing disc. *Development* **141**, 2339-2348.
Heller, D., Hoppe, A., Restrepo, S., Gatti, L., Tournier, A. L., Tapon, N., Basler, K. and Mao, Y. (2016). EpiTools: an open-source image analysis toolkit for quantifying epithelial growth dynamics. *Dev. Cell* **36**, 103-116.
Herboso, L., Oliveira, M. M., Talamillo, A., Pérez, C., González, M., Martín, D., Sutherland, J. D., Shingleton, A. W., Mirth, C. K. and Barrio, R. (2015). Ecdysone promotes growth of imaginal discs through the regulation of Thor in D. melanogaster. *Sci. Rep.* **5**, 12383.
Honegger, B., Galic, M., Köhler, K., Wittwer, F., Brogiolo, W., Hafen, E. and Stocker, H. (2008). Imp-L2, a putative homolog of vertebrate IGF-binding protein 7, counteracts insulin signaling in Drosophila and is essential for starvation resistance. *J. Biol.* **7**, 10.
Huang, J., Zhou, W., Dong, W., Watson, A. M. and Hong, Y. (2009). Directed, efficient, and versatile modifications of the Drosophila genome by genomic engineering. *Proc. Natl. Acad. Sci. USA* **106**, 8284-8289.
Jaiswal, M., Agrawal, N. and Sinha, P. (2006). Fat and Wingless signaling oppositely regulate epithelial cell-cell adhesion and distal wing development in Drosophila. *Development* **133**, 925-935.
Kakanj, P., Moussian, B., Grönke, S., Bustos, V., Eming, S. A., Partridge, L. and Leptin, M. (2016). Insulin and TOR signal in parallel through FOXO and S6K to promote epithelial wound healing. *Nat. Commun.* **7**, 12972.
Kim, D., Pertea, G., Trapnell, C., Pimentel, H., Kelley, R. and Salzberg, S. L. (2013). TopHat2: accurate alignment of transcriptomes in the presence of insertions, deletions and gene fusions. *Genome Biol.* **14**, R36.
Kozlova, T. and Thummel, C. S. (2000). Steroid regulation of postembryonic development and reproduction in Drosophila. *Trends Endocrinol. Metab.* **11**, 276-280.
Lavrynenko, O., Rodenfels, J., Carvalho, M., Dye, N. A., Lafont, R., Eaton, S. and Shevchenko, A. (2015). The ecdysteroidome of Drosophila: influence of diet and development. *Development* **142**, 3758-3768.
Lee, J. H., Budanov, A. V., Park, E. J., Birse, R., Kim, T. E., Perkins, G. A., Ocorr, K., Ellisman, M. H., Bodmer, R., Bier, E. et al. (2010). Sestrin as a feedback inhibitor of TOR that prevents age-related pathologies. *Science* **327**, 1223-1228.
Legoff, L., Rouault, H. and Lecuit, T. (2013). A global pattern of mechanical stress polarizes cell divisions and cell shape in the growing Drosophila wing disc. *Development* **140**, 4051-4059.
Li, L., Edgar, B. A. and Grewal, S. S. (2010). Nutritional control of gene expression in Drosophila larvae via Tor, Myc and a novel cis-regulatory element. *BMC Cell Biol.* **11**, 7.
Mao, Y., Rauskolb, C., Cho, E., Hu, W.-L., Hayter, H., Minihan, G., Katz, F. N. and Irvine, K. D. (2006). Dachs: an unconventional myosin that functions downstream of Fat to regulate growth, affinity and gene expression in Drosophila. *Development* **133**, 2539-2551.
Mao, Y., Tournier, A. L., Bates, P. A., Gale, J. E., Tapon, N. and Thompson, B. J. (2011). Planar polarization of the atypical myosin Dachs orients cell divisions in Drosophila. *Genes Dev.* **25**, 131-136.
Mao, Y., Tournier, A. L., Hoppe, A., Kester, L., Thompson, B. J. and Tapon, N. (2013). Differential proliferation rates generate patterns of mechanical tension that orient tissue growth. *EMBO J.* **32**, 2790-2803.
Marois, E., Mahmoud, A. and Eaton, S. (2006). The endocytic pathway and formation of the Wingless morphogen gradient. *Development* **133**, 307-317.
Martin, M. (2011). Cutadapt removes adapter sequences from high-throughput sequencing reads. *EMBnet. J.* **17**, 10-12.
Merkel, M., Sagner, A., Gruber, F. S., Etournay, R., Blasse, C., Myers, E., Eaton, S. and Jülicher, F. (2014). The balance of prickle/spiny-legs isoforms controls the amount of coupling between core and fat PCP systems. *Curr. Biol.* **24**, 2111-2123.
Merkel, M., Etournay, R., Popović, M., Salbreux, G., Eaton, S. and Jülicher, F. (2017). Triangles bridge the scales: quantifying cellular contributions to tissue deformation. *Phys. Rev. E* **95**, 032401.
Micchelli, C. A. and Blair, S. S. (1999). Dorsoventral lineage restriction in wing imaginal discs requires Notch. *Nature* **401**, 473-476.
Micchelli, C. A., Rulifson, E. J. and Blair, S. S. (1997). The function and regulation of cut expression on the wing margin of Drosophila: Notch, Wingless and a dominant negative role for Delta and Serrate. *Development* **124**, 1485-1495.
Milan, M., Campuzano, S. and Garcia-Bellido, A. (1996). Cell cycling and patterned cell proliferation in the Drosophila wing during metamorphosis. *Proc. Natl. Acad. Sci. USA* **93**, 11687-11692.
Milner, M. J. (1977). The eversion and differentiation of Drosophila melanogaster leg and wing imaginal discs cultured in vitro with an optimal concentration of beta-ecdysone. *J. Embryol. Exp. Morphol.* **37**, 105-117.
Mirth, C. K., Truman, J. W. and Riddiford, L. M. (2009). The ecdysone receptor controls the post-critical weight switch to nutrition-independent differentiation in Drosophila wing imaginal discs. *Development* **136**, 2345-2353.
Mitchell, N. C., Lin, J. I., Zaytseva, O., Cranna, N., Lee, A. and Quinn, L. M. (2013). The Ecdysone receptor constrains wingless expression to pattern cell cycle across the Drosophila wing margin in a Cyclin B-dependent manner. *BMC Dev. Biol.* **13**, 28.
Okamoto, N., Nakamori, R., Murai, T., Yamauchi, Y., Masuda, A. and Nishimura, T. (2013). A secreted decoy of InR antagonizes insulin/IGF signaling to restrict body growth in Drosophila. *Genes Dev.* **27**, 87-97.
Olson, C. M., Donovan, M. R., Spellberg, M. J. and Marr, M. T.II. (2013). The insulin receptor cellular IRES confers resistance to eIF4A inhibition. *Elife* **2**, e00542.
Ono, H., Rewitz, K. F., Shinoda, T., Itoyama, K., Petryk, A., Rybczynski, R., Jarcho, M., Warren, J. T., Marqués, G., Shimell, M. J. et al. (2006). Spook and Spookier code for stage-specific components of the ecdysone biosynthetic pathway in Diptera. *Dev. Biol.* **298**, 555-570.
Pastor-Pareja, J. C. and Xu, T. (2011). Shaping cells and organs in Drosophila by opposing roles of fat body-secreted Collagen IV and perlecan. *Dev. Cell* **21**, 245-256.
Preibisch, S., Saalfeld, S. and Tomancak, P. (2009). Globally optimal stitching of tiled 3D microscopic image acquisitions. *Bioinformatics* **25**, 1463-1465.
Puig, O., Marr, M. T., Ruhf, M. L. and Tjian, R. (2003). Control of cell number by Drosophila FOXO: downstream and feedback regulation of the insulin receptor pathway. *Genes Dev.* **17**, 2006-2020.

Development (2017) 144, 4406-4421 doi:10.1242/dev.155069

Resino, J., Salama-Cohen, P. and Garcia-Bellido, A. (2002). Determining the role of patterned cell proliferation in the shape and size of the Drosophila wing. *Proc. Natl. Acad. Sci. USA* **99**, 7502-7507.

Rogulja, D., Rauskolb, C. and Irvine, K. D. (2008). Morphogen control of wing growth through the Fat signaling pathway. *Dev. Cell* **15**, 309-321.

Rulifson, E. J., Micchelli, C. A., Axelrod, J. D., Perrimon, N. and Blair, S. S. (1996). wingless refines its own expression domain on the Drosophila wing margin. *Nature* **384**, 72-74.

Rulifson, E. J., Kim, S. K. and Nusse, R. (2002). Ablation of insulin-producing neurons in flies: growth and diabetic phenotypes. *Science* **296**, 1118-1120.

Sagner, A., Merkel, M., Aigouy, B., Gaebel, J., Brankatschk, M., Jülicher, F. and Eaton, S. (2012). Establishment of global patterns of planar polarity during growth of the Drosophila wing epithelium. *Curr. Biol.* **22**, 1296-1301.

Schindelin, J., Arganda-Carreras, I., Frise, E., Kaynig, V., Longair, M., Pietzsch, T., Preibisch, S., Rueden, C., Saalfeld, S., Schmid, B. et al. (2012). Fiji: an open-source platform for biological-image analysis. *Nat. Methods* **9**, 676-682.

Schwank, G., Tauriello, G., Yagi, R., Kranz, E., Koumoutsakos, P. and Basler, K. (2011). Antagonistic growth regulation by Dpp and Fat drives uniform cell proliferation. *Dev. Cell* **20**, 123-130.

Strassburger, K., Lorbeer, F. K., Lutz, M., Graf, F., Boutros, M. and Teleman, A. A. (2017). Oxygenation and adenosine deaminase support growth and proliferation of ex vivo cultured Drosophila wing imaginal discs. *Development* **144**, 2529-2538.

Teleman, A. A., Hietakangas, V., Sayadian, A. C. and Cohen, S. M. (2008). Nutritional control of protein biosynthetic capacity by insulin via Myc in Drosophila. *Cell Metab.* **7**, 21-32.

Trapnell, C., Roberts, A., Goff, L., Pertea, G., Kim, D., Kelley, D. R., Pimentel, H., Salzberg, S. L., Rinn, J. L. and Pachter, L. (2012). Differential gene and transcript expression analysis of RNA-seq experiments with TopHat and Cufflinks. *Nat. Protoc.* **7**, 562-578.

Tsao, C.-K., Ku, H.-Y., Lee, Y.-M., Huang, Y.-F. and Sun, Y. H. (2016). Long term *ex vivo* culture and live imaging of Drosophila larval imaginal discs. *PLoS ONE* **11**, e0163744.

Waddington, C. H. (1940). The genetic control of wing development in Drosophila. *J. Genet.* **41**, 75-113.

Weaire, D. and Rivier, N. (1984). Soap, cells and statistics – random patterns in 2 dimensions. *Contemp. Phys.* **25**, 59-99.

Worley, M. I., Setiawan, L. and Hariharan, I. K. (2013). TIE-DYE: a combinatorial marking system to visualize and genetically manipulate clones during development in Drosophila melanogaster. *Development* **140**, 3275-3284.

Wu, X. and Chen, D. Z. (2002). *Optimal Net Surface Problems with Applications*. Berlin; Heidelberg: Springer.

Yan, D. and Lin, X. (2009). Shaping morphogen gradients by proteoglycans. *Cold Spring Harb Perspect Biol* **1**, a002493.

Yoshiyama, T., Namiki, T., Mita, K., Kataoka, H. and Niwa, R. (2006). Neverland is an evolutionally conserved Rieske-domain protein that is essential for ecdysone synthesis and insect growth. *Development* **133**, 2565-2574.

Yu, G., Wang, L.-G., Han, Y. and He, Q.-Y. (2012). clusterProfiler: an R package for comparing biological themes among gene clusters. *OMICS* **16**, 284-287.

Zartman, J., Restrepo, S. and Basler, K. (2013). A high-throughput template for optimizing Drosophila organ culture with response-surface methods. *Development* **140**, 667-674.

Supplemental Materials and Methods

Analysis of hormone-responsive genesets

Using our selection criteria for hormone responsive genes, we expect that we are only isolating hormone-dependent genes and not genes that change over developmental time or in culture in a way that is independent of hormonal content. If the expression of a particular gene increases over time (independent of insulin or 20E), for example, we would expect to see its expression at the beginning of the experiment (no culture) be lower than its expression at 4 hrs under all conditions (no hormone, insulin or 20E). This gene would not, however, be identified as hormone responsive, since its expression in culture without hormone must differ from its level in culture with either insulin or 20E.

Nonetheless, it is possible that the progression of time and/or developmental progression could affect differences in expression levels that we observe in the hormone-responsive genesets at 4hr vs 9hr. For example, in Fig 4, we show that some genes have a stronger response to 20E at 9hr than at 4hr. It is possible that over developmental time, the expression of these genes may increase and that this increase over time in culture reflects a natural developmental progression. At the moment we have no way of controlling for these situations, because we only performed the transcriptomics on uncultured discs from animals of one timepoint. As another example, we identified a small group of genes whose expression after 4hr of culture in any condition is different from that of uncultured discs but recovers by 9hr to become closer to uncultured (96hr AEL) levels, both in insulin and in 20E. Because we chose to identify genes that were specific/common to 20E and insulin by comparing genes that were regulated at 9hr by 20E and 4hr by insulin, 11 genes that fit this pattern were falsely identified as being 20E-responsive (responding equally well to insulin or 20E at 9hr but to neither at 4hr). These genes were filtered out of our heatmaps in Fig. 5.

The functional classifications used in Fig. S6 and Fig. 5 are explained as follows: DNA replication/cell cycle includes anything having a positive effect on DNA replication and/or cell cycle progression. Cell death/DNA damage includes genes annotated with a function in apoptosis, programmed cell death, or DNA repair. Protein production includes splicing, translation, ribosome biogenesis, and protein folding. Nutrient transport was limited to proven or predicted members of the SLC/MFS superfamily. The patterning group includes anything known to regulate or be a target of developmental signaling pathways (in any system, not limited to the wing disc). The transcription/chromatin class included verified and putative transcription factors and chromatin modifying proteins. Tissue morphogenesis includes genes involved in cell-cell or cell-ECM contact, as well as cytoskeletal components and regulators. Lastly, the sugar modifications group describes anything involved in protein glycosylation.

Immunofluorescence

Discs were fixed for 20min at room temperature in 4% PFA/PBS. Samples were permeabilized by rinsing twice with PBS+0.1% TritonX100 (TPBS) and blocked with TPBS +0.1mg/ml BSA + 250mM NaCl for 45-60min at room temperature. They were then incubated overnight at 4˚C in primary antibody solution made in PBS+0.1% TritonX100+0.1mg/ml Bovine Serum Albumin (BBX). The next day, stainings were washed in BBX, followed by BBX+4% normal goat serum. Samples were then incubated at room temperature for 2-4hr in the dark with secondary antibodies diluted in BBX. Finally, samples were washed several times in TPBS and mounted between a glass slide and coverglass separated by a double-sided tape spacer. The discs were oriented with their apical surface toward the coverglass and immersed in VectaShield mounting medium (Vector Laboratories H-1000).

Development • Supplementary information

Analysis of live imaging

Analysis of cellular contributions to changes in tissue size and shape

The plots of accumulated local tissue shear presented in Fig. 7A and S11 were generated using a Eulerian approach. A fixed grid containing elements of 72 pixels (~14µm) wide was drawn over the tracked tissue region. At each timepoint, cells were assigned to the grid element based on the position of its center. Tissue shear (and its cellular contributions) was calculated from one frame to the next and averaged within each grid element. We then accumulated the average shear contained within each grid element from 2hr (after the adaptation phase) to the end of the movie. For this calculation, we considered only grid elements that have triangles covering more than half of the grid element area at a timepoint.

We quantify the relative area change rate and shear rate, averaged in the tracked wing pouch region, and the corresponding cellular contributions using the Triangle Method (Merkel et al., 2017). The relative area change decomposition states

$$v = \frac{1}{a}\frac{da}{dt} + k_d - k_e,$$

where a is the average cell area and k_d and k_e are cell division and extrusion rates. The relative area change rate v corresponds to the trace of the velocity gradient tensor $\partial_i v_j$. The indices i and j take values x and y. In Fig. 7Bi, we plot the accumulated relative area change of the tracked region of the wing pouch $\int_0^t v\,dt$ (blue line), accumulated relative change of the average cell area $\int_0^t \frac{1}{a}\frac{da}{dt}\,dt$ (green line), accumulated contribution due to cell divisions $\int_0^t k_d\,dt$ (orange line) and the accumulated contribution due to cell extrusions $\int_0^t k_e\,dt$ (cyan line).

The decomposition of the shear rate into its cellular contributions is

$$\tilde{v}_{ij} = \frac{DQ_{ij}}{Dt} + T_{ij} + C_{ij} + E_{ij} + D_{ij}\ ,$$

where Q_{ij} is the cell elongation tensor and D/Dt is a corotational derivative (Merkel et al., 2017). T_{ij}, C_{ij}, E_{ij} and D_{ij} are contributions to the shear rate from T1 transitions, cell divisions, cell extrusions and correlation effects, respectively. In Fig. 7Bii we plot the accumulated xx component of shear of the tracked region $\int_{t_0}^t \tilde{v}_{xx}\,dt$ (blue line), accumulated xx component of shear due to cell elongation change $\int_{t_0}^t \frac{DQ_{xx}}{Dt}\,dt$ (green line), accumulated xx component of shear due to T1 transitions $\int_{t_0}^t T_{xx}\,dt$ (red line), accumulated xx component of shear due to cell divisions $\int_{t_0}^t C_{xx}\,dt$ (orange line), accumulated xx component of shear due to cell extrusions $\int_{t_0}^t E_{xx}\,dt$ (cyan line) and accumulated xx component of shear due to correlation effects $\int_{t_0}^t D_{xx}\,dt$ (magenta line). The x-axis of the coordinate system is parallel to the DV boundary as explained in the main text. The initial timepoint is $t_0 = 2$hr.

The expansion of the wing pouch along the x-axis and the expansion along y-axis perpendicular to it are quantitatively described by velocity gradient components $\partial_x v_x$ and $\partial_y v_y$, respectively. These components of the velocity gradient tensor are determined from v and $\tilde{v}_{xx}$ as

$$\partial_x v_x = \frac{1}{2}v + \tilde{v}_{xx}$$

$$\partial_y v_y = \frac{1}{2}v - \tilde{v}_{xx}\ .$$

Development • Supplementary information

We then decompose the velocity gradient components into cellular contributions using the decompositions of v and $\tilde{v}_{xx}$ as follows

$$\partial_x v_x = \left(\frac{1}{2}\frac{1}{a}\frac{da}{dt} + \frac{DQ_{xx}}{Dt}\right) + T_{xx} + \left(\frac{1}{2}k_d + C_{xx}\right) + \left(\frac{1}{2}k_e + E_{xx}\right) + D_{xx}\,,$$

$$\partial_y v_y = \left(\frac{1}{2}\frac{1}{a}\frac{da}{dt} - \frac{DQ_{xx}}{Dt}\right) - T_{xx} + \left(\frac{1}{2}k_d - C_{xx}\right) + \left(\frac{1}{2}k_e - E_{xx}\right) - D_{xx}\,.$$

Here, $\frac{1}{2}\frac{1}{a}\frac{da}{dt} \pm \frac{DQ_{xx}}{Dt}$, $\pm T_{xx}$, $\frac{1}{2}k_d \pm C_{xx}$, $\frac{1}{2}k_e \pm E_{xx}$ and $\pm D_{xx}$ are the contributions to the velocity gradient component from cell shape change, T1 transitions, cell divisions, cell extrusions and correlations, respectively. The upper sign is used in the decomposition of $\partial_x v_x$ and lower sign in the decomposition of $\partial_y v_y$.

In Fig. 7Biii we plot the accumulated wing pouch expansion along the x-axis $\int_{t_0}^{t} \partial_x v_x\, dt$ (blue line), accumulated cell shape expansion along the x-axis $\int_{t_0}^{t} \left(\frac{1}{2}\frac{1}{a}\frac{da}{dt} + \frac{DQ_{xx}}{Dt}\right) dt$ (green line), accumulated contribution to the expansion along the x-axis due to T1 transitions $\int_{t_0}^{t} T_{xx}\, dt$ (red line), accumulated contribution to the expansion along the x-axis due to cell divisions $\int_{t_0}^{t} \left(\frac{1}{2}k_d + C_{xx}\right) dt$ (orange line), accumulated contribution to the expansion along the x-axis due to cell extrusions $\int_{t_0}^{t} \left(\frac{1}{2}k_e + E_{xx}\right) dt$ (cyan line) and accumulated contribution to the expansion along the x-axis due to correlation effects $\int_{t_0}^{t} D_{xx}\, dt$ (magenta line).

In Fig. 7Biv, we plot the accumulated wing pouch expansion along the y-axis $\int_{t_0}^{t} \partial_y v_y\, dt$ (blue line), accumulated cell shape expansion along the y-axis $\int_{t_0}^{t} \left(\frac{1}{2}\frac{1}{a}\frac{da}{dt} - \frac{DQ_{xx}}{Dt}\right) dt$ (green line), accumulated contribution to the expansion along the y-axis due to T1 transitions $\int_{t_0}^{t} -T_{xx} dt$ (red line), accumulated contribution to the expansion along the y-axis due to cell divisions $\int_{t_0}^{t} \left(\frac{1}{2}k_d - C_{xx}\right) dt$ (orange line), accumulated contribution to the expansion along the y-axis due to cell extrusions $\int_{t_0}^{t} \left(\frac{1}{2}k_e - E_{xx}\right) dt$ (cyan line) and accumulated contribution to the expansion along the y-axis due to correlation effects $\int_{t_0}^{t} -D_{xx}\, dt$ (magenta line).

In both Fig. 7Biii and Fig. 7Biv the initial timepoint is $t_0 = 2$hr.

Estimation of tracking errors

Even if the cells are perfectly segmented in each frame of the timelapse, the automated cell tracking can still produce errors in tracking. These errors include false positive and false negative divisions, false positive extrusions and false positive cell appearances. The tracking errors either falsely remove or add a cell to the tissue. Since the overall cell number does not depend on the precision of tracking, the tracking errors always appear in pairs. For example, if a cell track is lost from frame 1 to 2, it is given a new cell ID in frame 2. This one error would cause the counting of a false extrusion (as the cell is thought to be lost in frame 1) and a false cell appearance (to account for the arrival of a new unique track in frame 2). Alternatively, the new cell ID in frame 2 could be attributed to a false cell division, if it is interpreted to be the daughter of a (false) division by a neighboring cell. These pairs of false cell events occur close to each other in space and

time. We use this property to identify the tracking errors and adjust our quantification of the cellular contributions to tissue area change accordingly.

We have never observed any insertion of new cells into the wing disc epithelium and we thus assume that any cell appearance, not associated with a cell division, is due to an error in either segmentation or tracking. We devised a method to independently identify candidates for false positive and false negative divisions using the fact that just before the division, the apical area of the cell increases significantly as the nucleus moves apically. We measure the maximal cell area and the ratio of maximal cell area to the average of the cell area throughout the timelapse for each cell. We then discriminate dividing and non-dividing cells by performing a k-means classification on these two variables (Jones, 2001-). One type of error that could not be identified by this method might occur if the original tracking identifies two cell divisions for the same cell where only one actually occurs. In these situations, when the divisions are separated by less than six frames, we take the later division to be true and the earlier one to be false. Using these candidates for dividing and non-dividing cells we construct a list of candidates for false positive and false negative divisions in the original tracking.

Finally, we pair cell appearances with cell extrusions and false negative cell division candidates, and then we pair the false positive cell division candidates with the remaining cell extrusions and remaining false negative cell division candidates. The cell events we manage to pair in this way we treat as false, and we adjust the cell event counting accordingly.

To construct pairs of these cell events where each event can appear at most once, we introduce a distance measure between cell events A and B in time and space:

$$d(A,B) = \sqrt{\frac{1}{2}(f_A - f_B)^2 + (x_A - x_B)^2 + (y_A - y_B)^2}$$

where $x_{A,B}$and $y_{A,B}$ are coordinates of the cell centers (in pixels) in frame $f_{A,B}$ of the cell event, for each of the two cell events. We then iteratively construct pairs of false cell events from all possible combinations by repeating the following steps:

find a cell event pair with minimum d(A,B)

- if d(A, B) > 25 stop the procedure
- if d(A, B) < 25 identify pair (A, B) as a pair of false cell events
- remove the events A and B from consideration in future iterations

This method identifies more than 90% of the cell appearances as false. It also finds that between 85-90% of cell divisions and 45-75% of cell extrusions initially identified by Tissue Analyzer were true events and that between 10-20% of true divisions were not recognized by Tissue Analyzer. We used the corrected numbers of cell divisions and extrusions to calculate contributions to tissue area change. The remaining number of cell appearances is very low (<10) in all three experiments and not shown in the relative area change plots. This method does not identify the daughter cells. Therefore, in the shear calculation by the Triangle Method, we used the original tracking by the Tissue Analyzer. If we assume that the errors in cell division tracking are not correlated with the cell division orientation and that the falsely identified cell divisions are not oriented on average, we can estimate the relative error of the shear due to cell divisions to be equal to the fraction of true division events not recognized by the Tissue Analyzer i.e. 10-20%.

Development • Supplementary information

Figure S1:
Lower 20E concentration does not prevent the arrest of proliferation in insulin

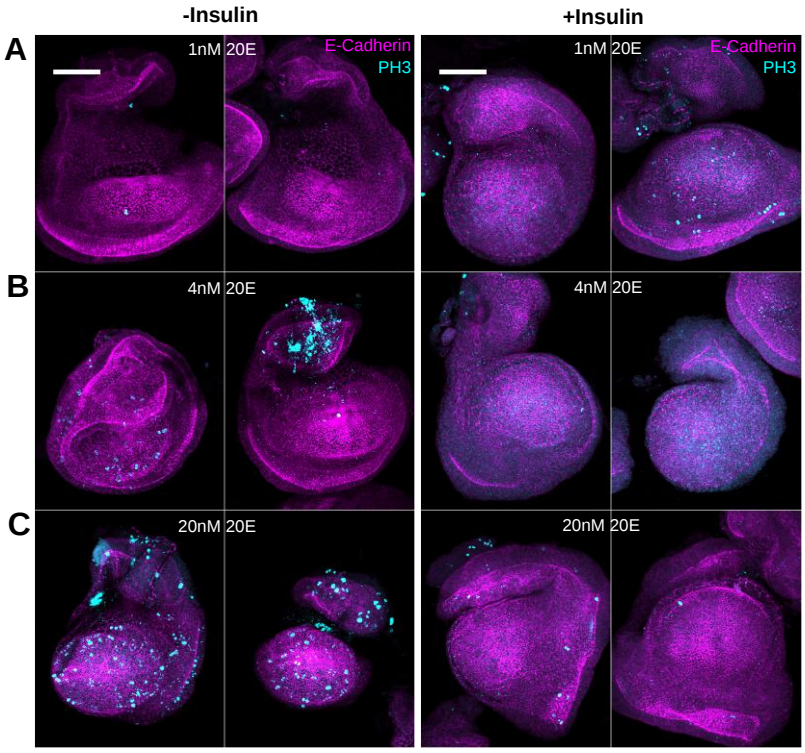

To determine whether lower concentrations of 20E would allow insulin to further improve proliferation, discs were cultured for 24hr in 1nM (A), 4nM (B) or 20nM (C) 20E, with or without 5ug/ml insulin (right/left, respectively). After this length of culture, discs start to lose their morphology, making quantification difficult. In particular in insulin (+/- 20E), the pouch region balloons forward and out. In all discs, the prospective notum starts to curl forward. Only in 20nM 20E alone (without insulin) is there any consistent division remaining. Best attempts were made to orient images with anterior to the left and dorsal up. Scale bar is 50um.

Development • Supplementary information

Figure S2:
Cellular component GO terms enriched in subgroups of insulin regulated genes

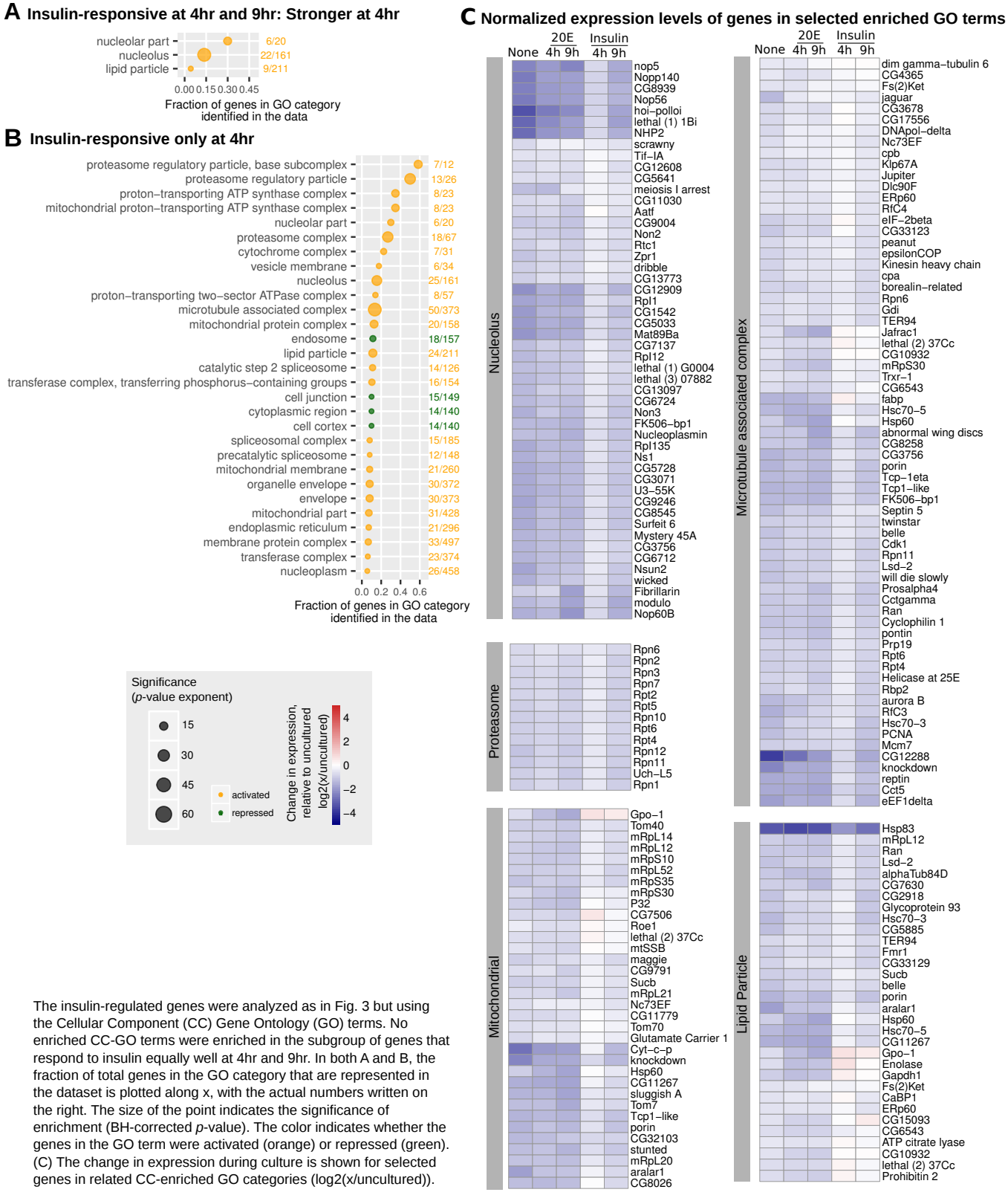

The insulin-regulated genes were analyzed as in Fig. 3 but using the Cellular Component (CC) Gene Ontology (GO) terms. No enriched CC-GO terms were enriched in the subgroup of genes that respond to insulin equally well at 4hr and 9hr. In both A and B, the fraction of total genes in the GO category that are represented in the dataset is plotted along x, with the actual numbers written on the right. The size of the point indicates the significance of enrichment (BH-corrected *p*-value). The color indicates whether the genes in the GO term were activated (orange) or repressed (green). (C) The change in expression during culture is shown for selected genes in related CC-enriched GO categories (log2(x/uncultured)).

Development • Supplementary information

Figure S3:
Known targets of TOR and FoxO transiently respond to insulin in cultured wing discs

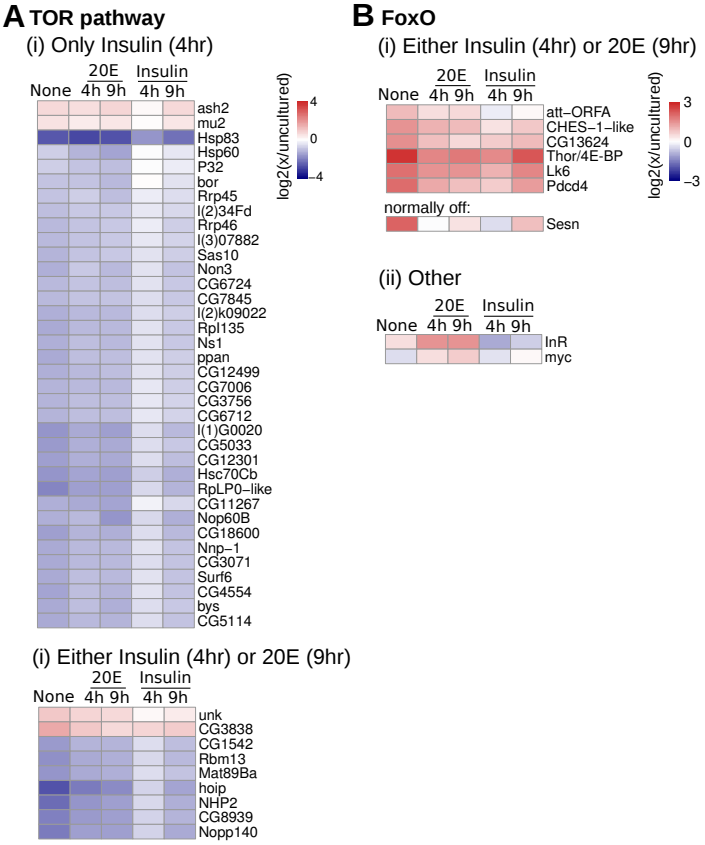

The expression levels of previously-identified TOR- (A) and FoxO-responsive (B) genes were examined in the dataset from wing discs cultured in insulin or 20E. Shown are the changes in expression from that in uncultured discs (log2(x/uncultured)). In (A), genes are grouped based on whether they respond to only insulin (i) or to either insulin or 20E (ii). In (B), most of the FoxO target genes were found to respond to both insulin (at 4hr) and 20E (at 9hr) (i). The *sesn* gene is normally not expressed in wing discs, but becomes upregulated in certain culture conditions. For this case, we report its change in expression relative to our minimum cutoff for expression (5 fpkm). We also show in (ii) values for the insulin receptor (*dInR*) and *myc*, which are thought to be FoxO targets.

Development • Supplementary information

Figure S4:
PI3K remains active throughout long term culture in insulin

A **PH-GFP reporter of PI3K activity during culture with insulin alone**

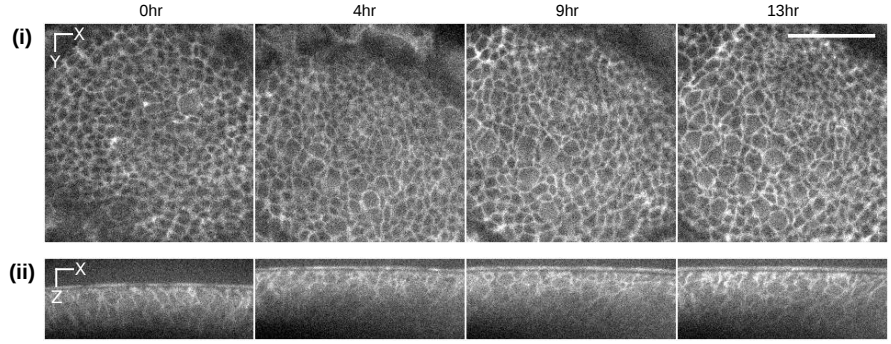

B **PH-GFP reporter of PI3K activity during culture without hormone**

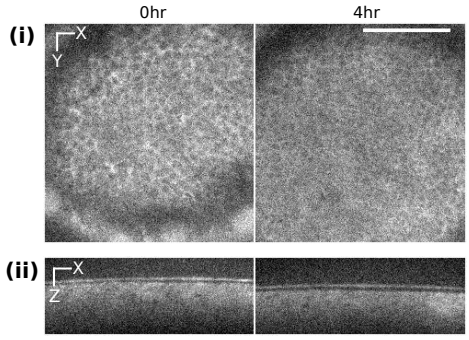

PH-GFP reporter of PI3K activity during culture with insulin (A) or no hormone (B). This reporter localizes to the membrane upon PIP3 production, thus reflecting PI3K activity. A single xy plane is shown in (i) and an xz slice through the middle of the disc is shown in (ii). Timepoints shown in each part are from the same disc grown on the microscope. Scale bar is 20um.

Development • Supplementary information

Figure S5:
Insulin causes cytoplasmic retention of FoxO, even after 9hr of culture

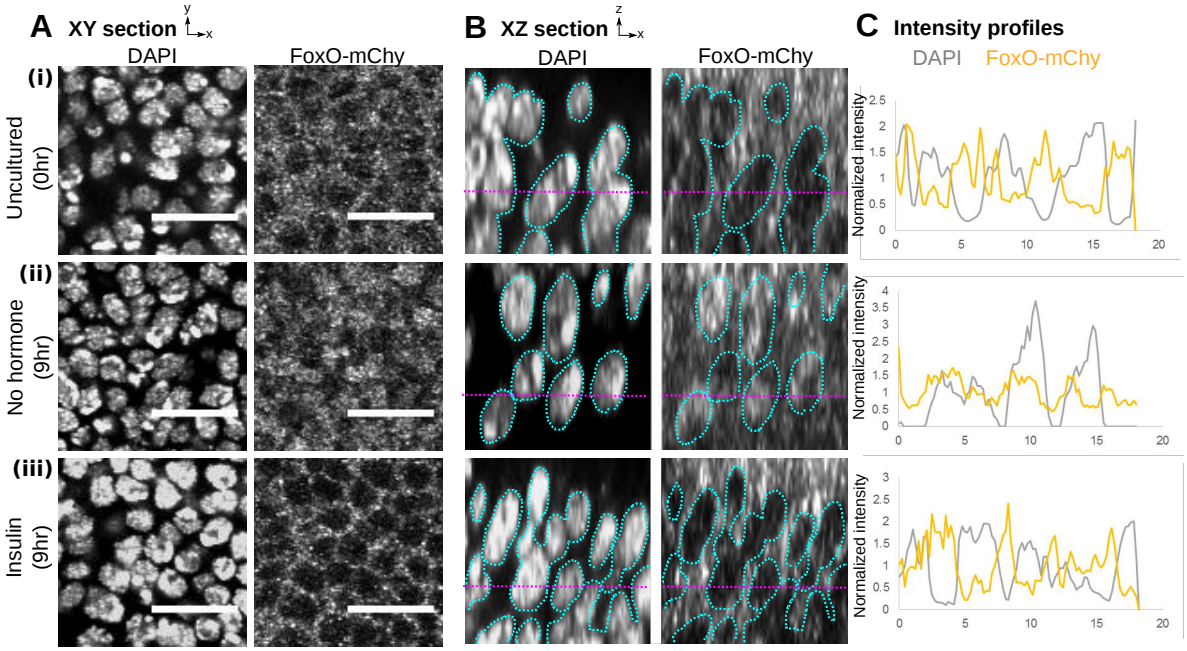

Wing discs from mid-third instar larvae expressing FoxO-mCherry were fixed either immediately after dissection (i) or after 9hr of culture in no hormone (ii) or insulin (iii). They were then stained with DAPI, to mark cell nuclei, and an antibody against mCherry, to mark the FoxO. Shown are single Z-planes (A) or zoomed-in XZ sections (B) from a region of the dorsal-anterior part of the wing pouch. In (B), blue dotted lines trace the outlines of nuclei on both images, and the purple dotted line is the location of the intensity values plotted in (C). In (C), the intensities of DAPI and FoxO-mCherry were normalized for each image to the average intensity of the channel along the line and plotted as a function of position. Scale bars in (A) are 10um.

Development • Supplementary information

Figure S6:
Overlap between insulin- and 20E-regulated genesets

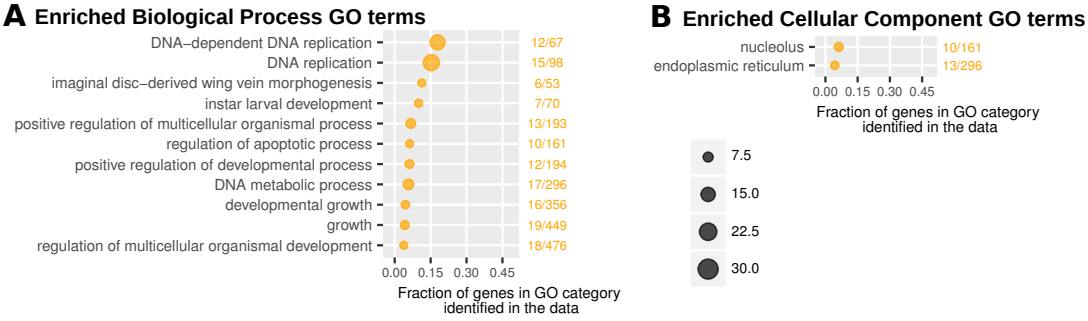

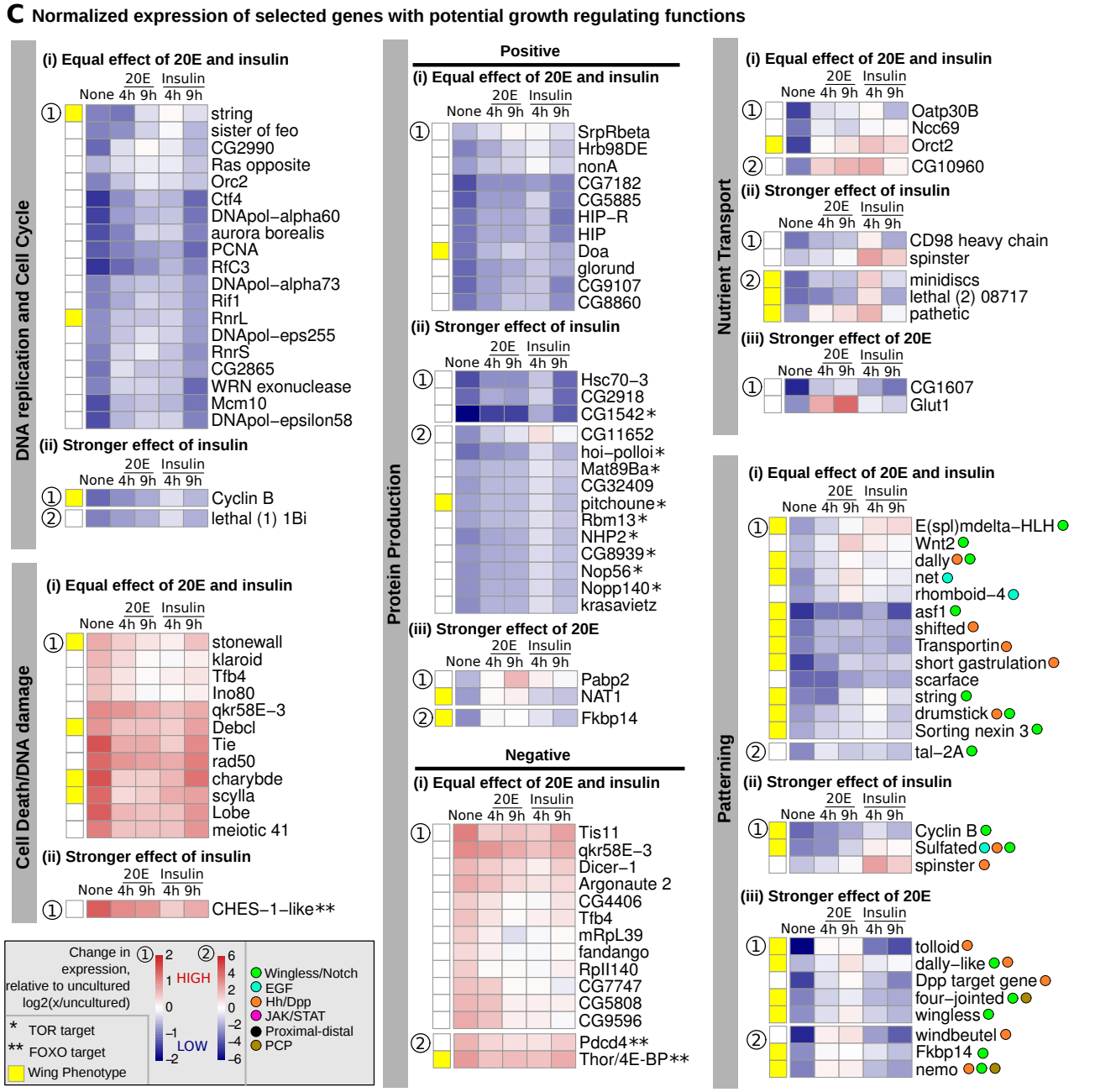

Enriched biological process (A) or cellular component (B) GO terms were identified in the set of genes regulated by both insulin (at 4hr) and 20E (at 9hr). Labels on the right indicate the number of genes in the data over total genes in that GO category. (C) The change in expression from that in uncultured discs (log2(x/uncultured) is shown for genes of selected functional categories. Genes in each group were further subdivided based on whether the two hormones had equal (i) or unequal effects (ii, insulin stronger vs iii, 20E stronger). Genes were plotted on one of two scales (labeled as 1 or 2), depending on how much their values changed across conditions. Yellow squares indicate known phenotypes in the wing (at any stage of development) for loss of function for genes positively regulated by hormone or gain of function for genes negatively regulated by hormone. Asterisks indicate previously identified TOR (*) or FOXO (**) targets.

Figure S7:
20E-signaling is autonomously required for wing growth during the third instar

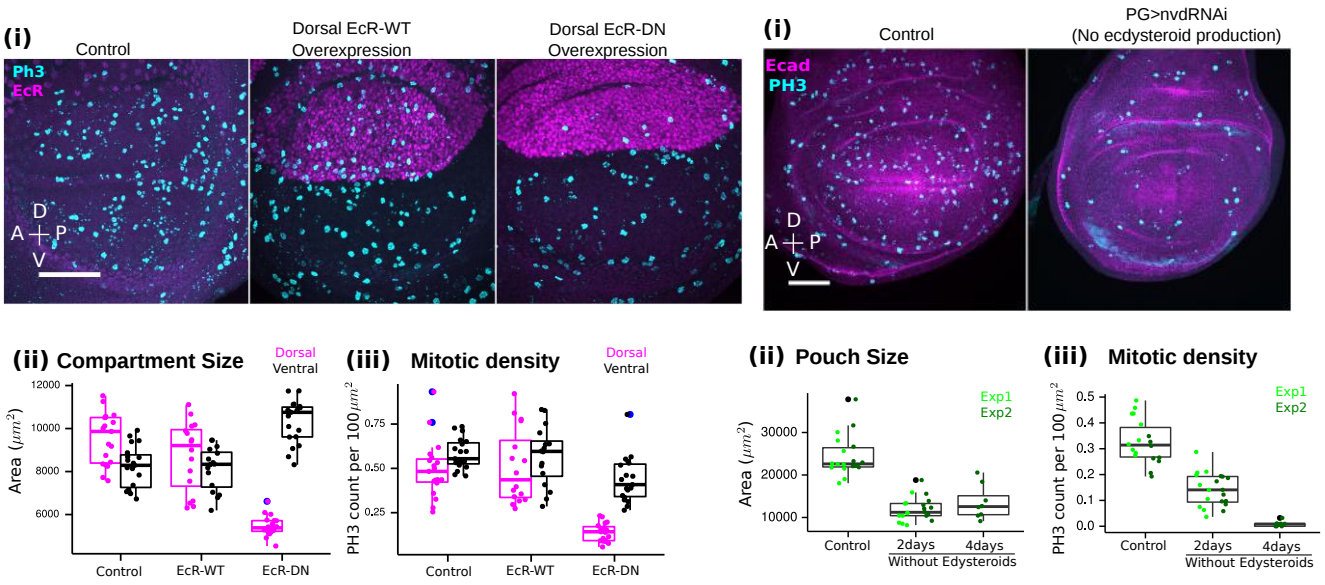

(A) *Apterous-GAL4*, which is expressed in the dorsal compartment of the wing disc, combined with *tub>GAL80ts* was used to overexpress either a wild type (EcR-WT, middle) or dominant negative allele of the Ecdysone Receptor (EcR-DN, right) for 24hr during the third instar. The negative control is the *apterous-GAL4, gal80ts* crossed to wild type (left). (i) Representative images show staining for phospho-Histone-H3 (PH3, a mitotic marker, cyan) as a maximum projection overlaid with EcR (magenta). (ii) Quantification of compartment size (dorsal=pink, ventral=black) was done by measuring area in a maximum projection image. (iii) Mitotic density was measured in the Dorsal (pink) and Ventral (black) compartments by counting number of PH3-positive nuclei per area.

(B) *Phantom-GAL4*, which is expressed in the prothoracic ecdysteroid-producing gland of the brain, combined with *tub>GAL80ts* was used to induce an RNAi targeting neverland (*nvd*) during the third instar. *Neverland* is required to synthesize ecdysteroids. Control larvae, containing only the *phantom-GAL4, tub>GAL80ts* crossed to wild type, formed pupae after 2 days at 29C; *nvd-RNAi* larvae stayed as larvae for several days. (i) Representative images show PH3 staining (cyan) as a maximum projection overlaid with E-cadherin (magenta). Pouch size (area in a maximum projection image, ii) and mitotic density (iii) were measured for the region surrounded by the innermost folds. Data from two independent replicates of the experiment are separately colored.

For both A and B: (i) Scale bar is 50um. In (ii) and (iii), each dot represents one disc, with bars showing the extent of the first and third quartiles; lines reach up to 1.5* IQR (interquartile range); outliers outside of this range are blue (left) or black (right) dots.

Development • Supplementary information

Figure S8:
20E-signaling is required in the posterior compartment for Wg expression

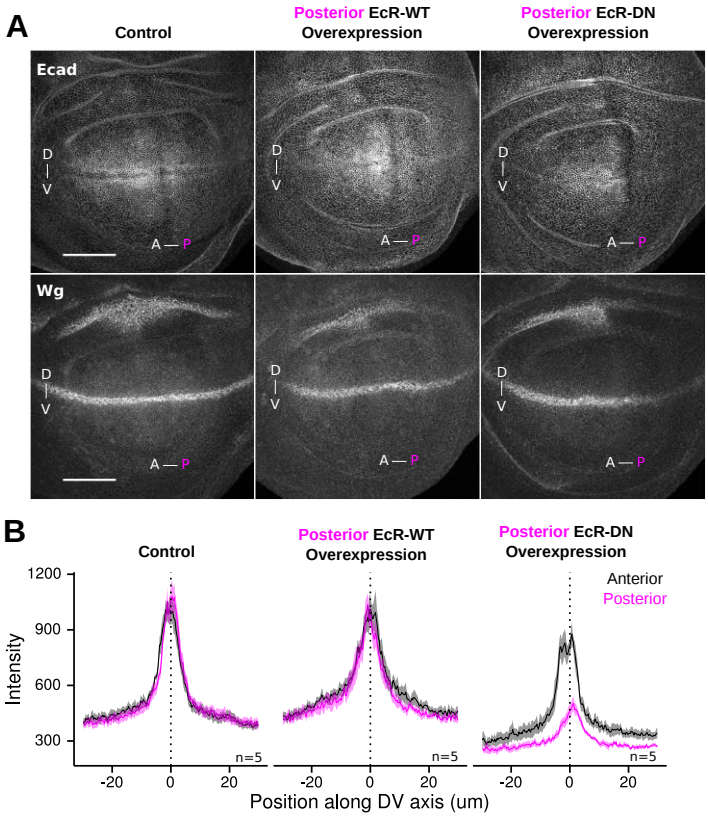

Engrailed-GAL4, which is active in the posterior wing disc, was combined with *tub>GAL80ts* to to transiently overexpress a dominant negative (EcR-DN, right) or wild type (EcR-WT, middle) allele of the Ecdysone Receptor for 24hr in the third instar. The control (left) was *engrailed-GAL4, tub>GAL80ts* crossed to wild type flies. (A) Representative images of E-Cadherin (top) or Wg (bottom) staining in the same discs. Dorsal is up, anterior to the left. Markers deliniate the boundaries. Scale bars are 50um. (B) Wg expression was quantified by measuring the absolute intensity alone a line drawn from Dorsal to Ventral of the pouch in the Anterior (black) or Posterior (pink) compartments. Shown is the mean (dark line) and standard deviation (shaded ribbon) of five discs. Control and perturbation stainings were done in parallel and imaged with the same acquisition settings on the same day.

Development • Supplementary information

Figure S9:
Circulating ecdysone is required for wing pattern during growth

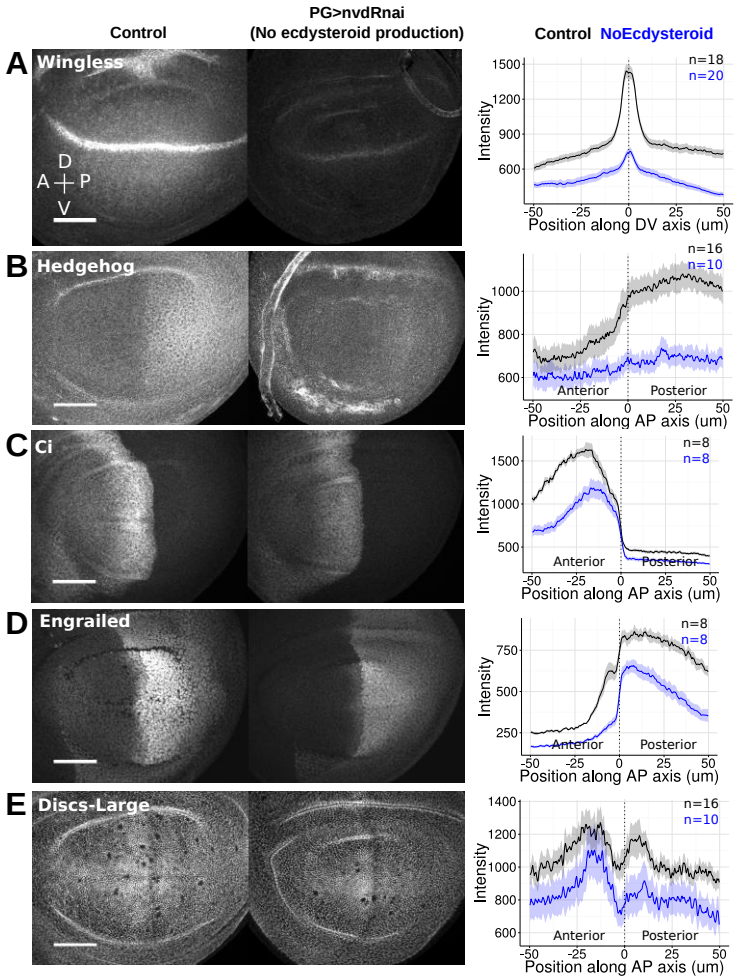

Phantom-GAL4, which is expressed in the prothoracic ecdysteroid-producing gland of the brain, combined with *tub>GAL80TS* was used to induce RNAi against *neverland* (*nvd*), a gene required to synthesize ecdysone, only during the third larval instar. Expression of Wingless (A), Hedgehog (B), Ci, the transcriptional activator downstream of Hh signaling (C), Engrailed, a Hh target gene (D), and Discs-large, a septate junction marker (E) was analyzed by immunofluorescence. Quantification of the changes in expression was performed by plotting the absolute intensity along a line drawn from one compartment to another. For (A), the line was drawn from Dorsal to Ventral in the Anterior comparment. For (B)-(E), the line was drawn from Anterior to Posterior in the Dorsal compartment. Black is the control; blue is the nvd-RNAi animals. The dark line is the mean for all discs measured in the same staining experiment; the shaded ribbon indicates the standard deviation. Control and perturbation stainings were done in parallel and imaged with the same acquisition settings on the same day. Scale bars correspond to 50um.

Development • Supplementary information

Figure S10:
Analysis of growth dynamics during live imaging was performed on a fully trackable region of the tissue

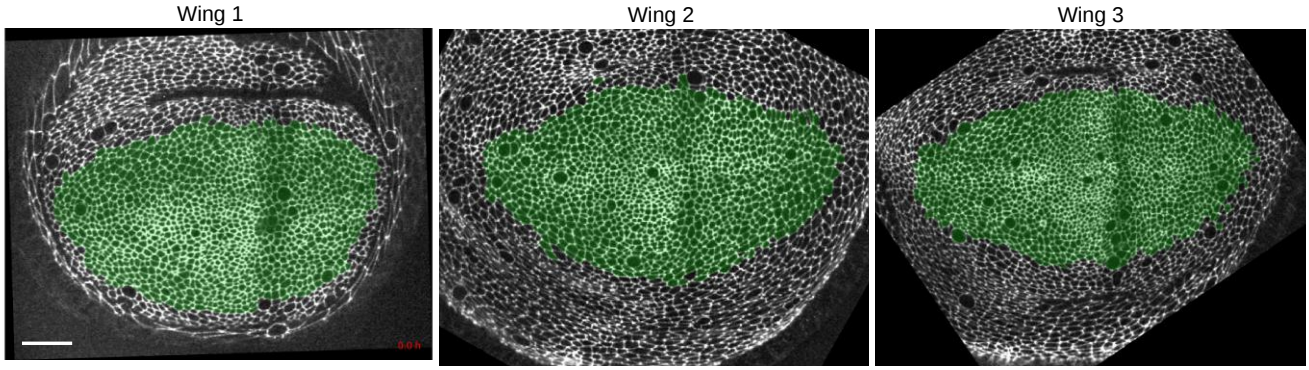

Shown are the first images of each analyzed movie, with green cells highlighting the region that is fully trackable for the length of the timelapse. This region will form the distal wing blade in the adult. Scale bar indicates 20um. Dorsal is up; anterior to the left.

Development • Supplementary information

Figure S11:
Patterns of total shear and its cellular contributions measured from live imaging

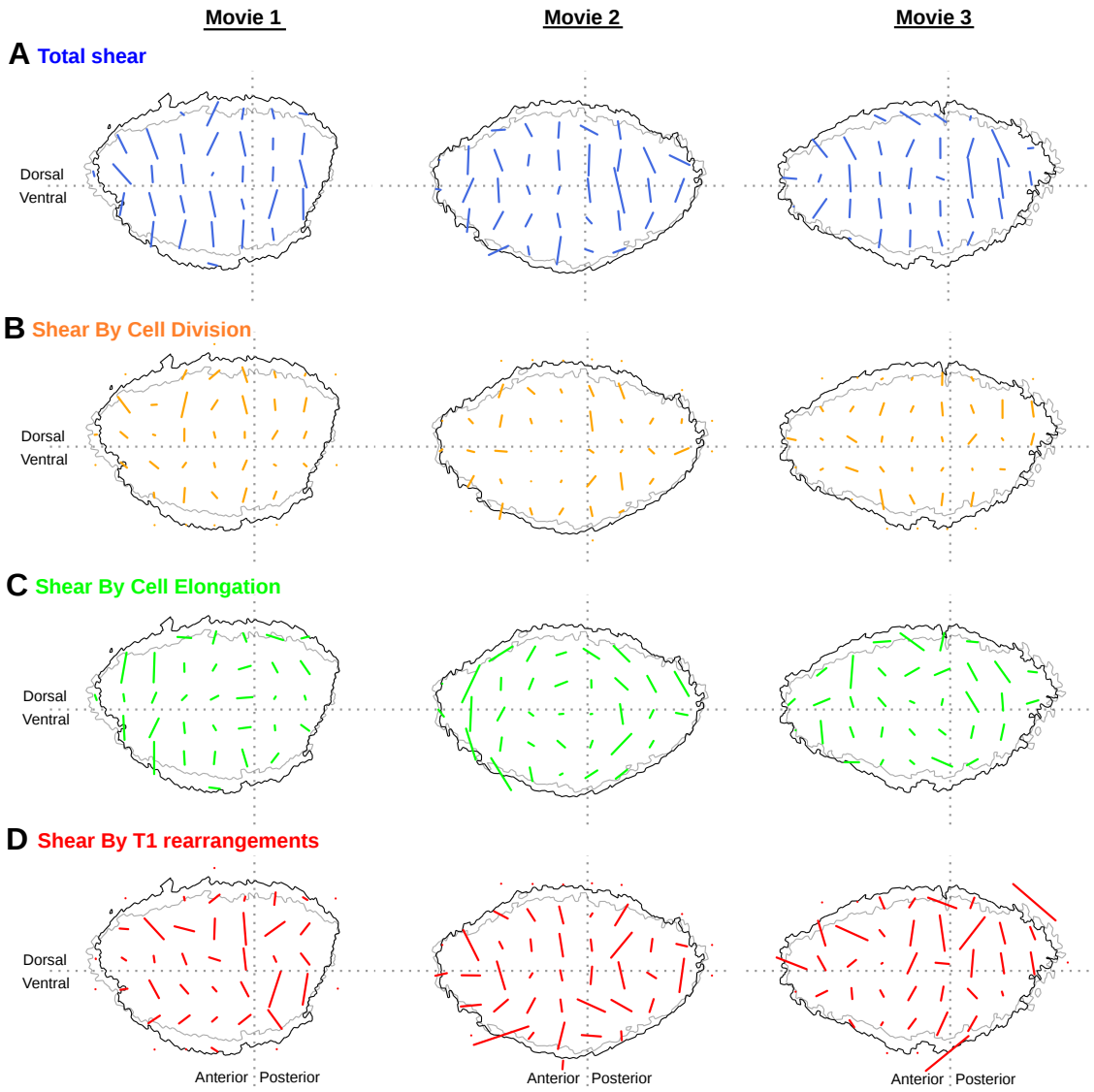

Three E-Cadherin-GFP-expressing wing discs were imaged for >13hr, and cells of the future wing blade region were segmented and tracked. Patterns of tissue shear were measured after the first 2hr adaption phase and are displayed on the outline of the analyzed tissue at the beginning (2hr, grey) and end (13.3hr, black) of the analyzed time window. To generate these shear patterns, we divided the tissue into grid, where each square has a width = 72 pixels. We calculated the area-weighted average tissue shear that occurred between two consecutive frames within each grid and then accumulated this value over time from 2-13hrs. The length of the bar is proportional to its magnitude and its orientation indicates its direction. Shown separately are the patterns for total shear (A, repeated here from Fig. 7A, in order to easily compare to the patterns of cellular contributions), and the contributions to this shear from cell divisions (B), cell elongation change (C), and T1 rearrangements (D).

Development • Supplementary information

Supplemental Table S1: List of genes regulated by Insulin at one or both timepoints

Click here to Download Table S1

Supplemental Table S2: List of genes regulated by 20E at one or both timepoints

Click here to Download Table S2

Supplemental Table S3: List of genes regulated at 4hr by insulin alone, 20E alone, or by either hormone

Click here to Download Table S3

Supplemental Table S4: List of genes regulated at 9hr by insulin alone, 20E alone, or by either hormone

Click here to Download Table S4

Supplemental Table S5: List of genes regulated by 4hr in insulin alone, 9hr in 20E alone, or by either hormone at these timepoints

Click here to Download Table S5

Supplemental Movie 1: Long term timelapses of wing discs cultured in 20E

Three E-cadherin-GFP-expressing wing discs were imaged in 20E-containing media, acquiring Z-stacks in a 2x2 tiling every 5 min. Shown are 2D projections of the pseudostratified wing pouch layer after tile stitching. Images were rotated and resized for presentation. Dorsal is up, anterior to the left. Frame rate is 10 frames per second.

Development • Supplementary information